UNIVERSITY OF OKLAHOMA GRADUATE COLLEGE

A MODERNIZED CUTDOWN/LETDOWN MECHANISM FOR MOBILE BALLOON LAUNCHES

A THESIS

SUBMITTED TO THE GRADUATE FACULTY

in partial fulfillment of the requirements for the

Degree of

MASTER OF SCIENCE

By

Christopher Schneider

Norman, Oklahoma

2025

A MODERNIZED CUTDOWN/LETDOWN MECHANISM FOR MOBILE BALLOON LAUNCHES

A THESIS APPROVED FOR THE

SCHOOL OF AEROSPACE AND MECHANICAL ENGINEERING

BY THE COMMITTEE CONSISTING OF

Dr. J.D. Baldwin, Chair

Dr. Michael Stock

Dr. Srikanth Bashetty

ACKNOWLEDGEMENTS

This thesis and graduate school journey were filled with a wealth of experiences and learning. I would like to take this moment to thank my gracious advisor Dr. Baldwin for his guidance and expertise throughout my research goals. The continual guidance for formatting, grammar and methods of analysis shoved me in the right direction to finish this document. I am grateful to Dr. Bashetty for pointing me in the direction of Dr. Baldwin and agreeing to be a part of my committee. I would like to thank Dr. Stock for guiding me in the correct direction of different federal guidelines, manufacturing methods, mathematical calculations, encouraging me to do everything how I see fit and keep me on pace. I would like to thank Dr. Chmielewski for always helping me organize my research goals and thoughts and discuss different methods of approach for this project.

I have had a wealth of experience with prototyping and manufacturing in large favor due to the Field Observing Facilities and Support team at NSSL. I would like to thank Dr. Waugh for taking me in as a student in undergrad and allowing me to experience the intersection of Engineering and Atmospheric Sciences. This has guided me in so many ways in both academic and career goals. I would like to thank Mr. Kennedy and Mr. Barney for always wanting to help with theoretical concepts, designs, 3D printer chats and much more.

I am eternally grateful to my family and friends for instilling an interest in pursuing my goals and constantly pushing what I am capable of. I was instilled with an interest of setting a good example of success in front of me and this has guided me both in life and throughout my academic journey.

Finally, I want to thank all the people who have helped me throughout my life to get to this point. There are so many influences on my life that I would like to thank but would not have the amount of time or pages to do so. To everyone who has helped me, thank you.

Table of Contents

List of Figures

List of Tables

ABSTRACT

Mobile balloon launches at The National Oceanic and Atmospheric Administration (NOAA) National Severe Storms Laboratory (NSSL) are vital for upper air data sources and in situ observations. Instruments such as the Electric Field Meter and the Particle Size, Imaging and Velocity probe are attached to balloons to investigate the local electric field and microphysical properties in storms where direct observations are sparse. To constrain the distance flown by the package, as well as limit potential damage sustained to sensors, a cutdown mechanism releases the instrument package from the balloon. The package also features a letdown system to increase the distance between the sensor package and balloon once in flight to reduce the influence of the balloon on the measurements. To enhance reliability and ensure compliance with Federal regulations, the existing system requires modernization. This research project presents a prototype hook and latch mechanism for the cutdown application ensuring ease of use and improved operational capabilities. The reverse engineering of a gear based spool mechanism for letdown application was carried out for ease of manufacturing and optimization of recovery efforts. Additionally, the project outlines the development process of a shear pin aligned with Federal guidelines to break at a given impact force of approximately 222 N (50 pounds). A comprehensive analysis of all designed geometries was carried out using Ansys engineering software for finite element analysis (FEA), SOLIDWORKS modeling, drop testing of parts, video analysis, and theoretical force calculations. The methodology presented in this study produces a successful mechanism optimized for deployment in various severe weather field applications.

Chapter 1. Introduction

Mobile weather balloon launches at the National Oceanic and Atmospheric Administration (NOAA) National Severe Storms Laboratory (NSSL) are particularly instrumental for in situ observations of upper air atmospheric phenomena. Providing a wealth of data, these flight missions are vital to obtaining a vertical structure of the atmosphere. Research objectives covered under this umbrella include severe and winter weather microphysical features, electric field disturbances, atmospheric stratification, and vertically integrated profiles. Depending on the research goals of a specific project, these flights may be modified. The variable nature of these flights makes them instrumental for atmospheric science as they provide valuable and often scarce data in an unsampled environment. Figure 1 displays a full suite of instrumentation and mechanisms for a successful electric field measurement flight.

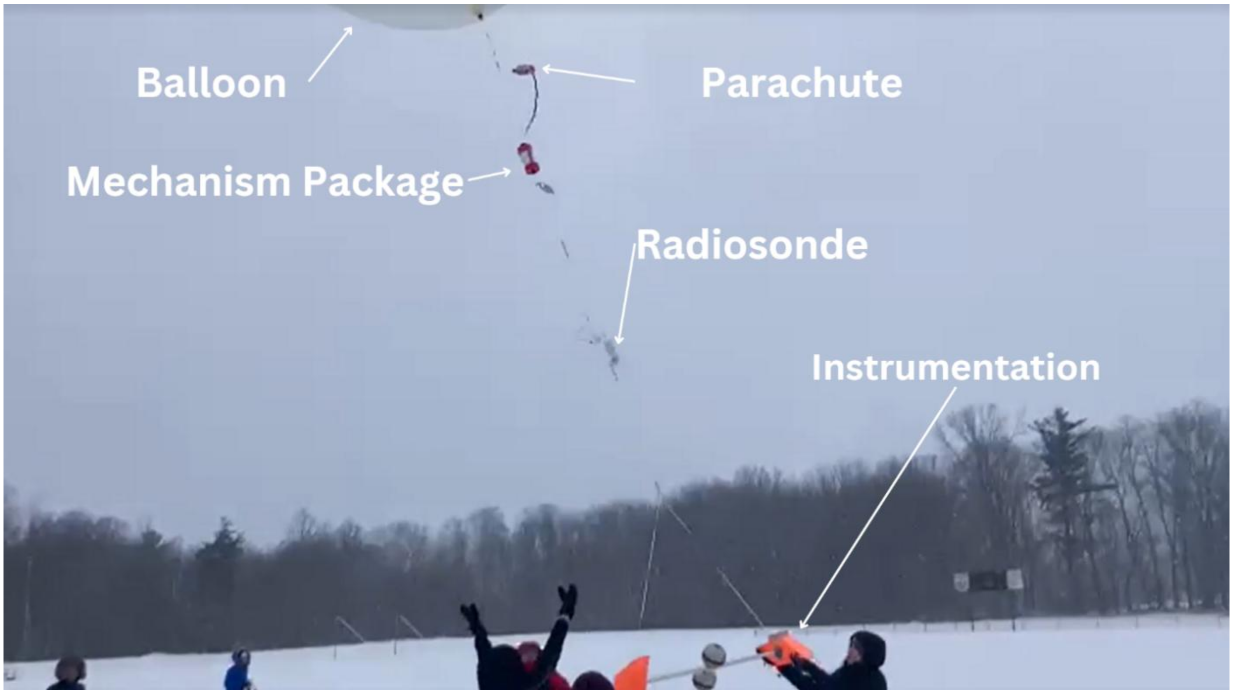

Figure 1: Components of a Full Suite of Instruments on a Data Acquisition Launch

The balloon train is composed of several integrated systems. The package that runs operations is a tubular shaped device containing a printed circuit board, satellite chip, GPS locater, and the cutdown and letdown mechanisms. The primary goal of this research project is the redesign of the cutdown and letdown systems. It is important to understand the distinction between these two mechanisms and the package into which they are assembled. The development of new mechanisms enhances the operation of these ballooning systems by enabling precise release and controlled distancing.

There are understood limitations to balloon flights, which present interesting questions relating to the observed data [1]. Influences from the ascending balloon create a wake that could negatively alter the data collected by the sensors. The issue arises while trying to prevent data readings that are accurate but do not properly represent the sampling environment through these wake zones. This bias must then be recognized in any corresponding data sets or publications creating more work on the latter side.

There are many methods to limit the effects of such quality disparity. Distancing the balloon from the instrument package is an effective way to restrict the wake influence and ensure a most effective flight. This proposed idea of a letdown is observed in many different instances of ballooning and is most often associated with radiosondes. The radiosonde is a battery powered instrument that uses telemetry to transmit its data. These packages are often small (< 20 cm), and the accompanying balloon is much smaller than those dealt with in this project.

The data collected by radiosondes is accordingly very susceptible to the influences of balloon wake. Data sources such as temperature, humidity, and even wind speed and direction can be altered by this wake presented by the ascending balloon. These letdown systems are often purchased from the accompanying manufacturer and reduced to two components: string and a spool.

While often assumed as a vertical measurement, these data acquisition flights often drift. It is most important to see that the balloon is released at the correct time to ensure that any horizontal movement can be aligned with the proposed sample environment. The instrument train is costly and therefore at times it is appropriate to release the package from the balloon to prevent further drifting.

1.1 Components Causing Issues

There are two components that are causing issues within the existing mechanism package. Breaking down the internals, there is a device that allows for distancing between the balloon and the instrumentation to reduce the influence of the wake caused by the balloon. There is a second mechanism responsible for releasing the instrument train completely from the balloon, ending the data mission. These mechanisms are referred to as the letdown and cutdown mechanisms respectively.

1.1.1 Letdown Mechanism

The letdown mechanism function begins at a predetermined time, often near the start of data acquisition and after the release of the balloon. The deployment of the spooled line must be precisely timed to prevent any component of the instrument train from becoming obstructed by the surrounding environment. This is important due to the presence of tree canopies, power lines, and occasional buildings. These obstructions can mean an immediate end to the mission at hand. The system uses a spooled line to extend the distance of the sensors from the ascending balloon. An operator is most often responsible for the activation of the spool. At times, most especially in the past, a timed circuit had been used for this purpose. A timed circuit can become troublesome if it does not trigger or takes too much time to trigger. The spool will then drop the instrument train roughly 30.4 meters (100 feet) using a load bearing braided line. The spool in Figure 2, is machined out of aluminum and uses this gear based system to slowly letdown the package.

Figure 2: Geared Letdown Mechanism

The manufacturer of the spool, Durable™, is not currently selling parts and therefore unable to acquire a new set of letdown reels. Alternative options are available on the market, but due to interest in manufacturing in house, this option was not explored. Figure 2 displays a used spool recovered after a data flight. This system must possess a controlled unreel function to prevent a higher dynamic jerk upon the tension of the line. This dynamic load could prove detrimental to the instrumentation as well as induce a strain on the line with the increased potential for failure. The evolution of these spools had displayed many different methods of controlled release. Failure modes were most evident in motorized mechanisms, where balancing weight and efficiency emerged as a key challenge. The motors often burned out or were jammed and not able to release the load. Other failure modes were observed through simplified mechanisms such as jamming, overstrained parts, and even tangling problems. A gear based spool, as shown in Figure 2, proved to be the most successful, but certainly is not without its issues such as manufacturing issues and the expected life of the mechanism.

An issue arises from the release of the package from the balloon in the form of a 30.4 meter line, often tangled in trees or powerlines. Retrieving the components is crucial, yet the line often becomes tangled in its surroundings making the recovery process significantly more challenging. This issue brings up a potential safety issue also with the concern that a slack line such as this could find itself crossing a highway or busy intersection.

The decision up to this point to ensure operations was to use the aged but most efficient geared spools from Figure 2. Repeatability then became a consistent issue and main interest in this project as these mechanisms were in limited supply. Problems such as wear and tear on reusable parts not allowing consecutive flights create issues in data collection where significant data events would potentially be missed due to the unavailability of the platforms.

1.1.1 Constraints for Letdown Mechanism

The aluminum machined geared letdown in Figure 2 proved to be unreliable for continual use as the gears began to show signs of degradation. The teeth carrying a load showed deformation and in some severe cases, showed no contact with the limiting bars. The slipping of the teeth meant the spool was allowed to free spin and some flights likely experienced a dynamic jerk which could have led to excessive dynamic strain and the potential for a failed flight. This jerk, represented by the change in acceleration per unit time, ($^{da}/_{dt}$), is the main initiator of failure for the manufactured parts. The selected material must either be stiff enough to sustain the load and/or be replaceable easily enough that subsequent flights are not hindered by a previous launch.

The material and mechanism must reliably withstand both shock loads and sustained loads consistent with the instrument train's operational conditions. At launch, a impulse pulls the package downward, adding to the static load that remains present throughout the balloon's flight.

Environmental factors also play a crucial role in material selection. It is well documented that temperature decreases with altitude [2], making thermal resilience a key consideration for material choice. The mechanism must function effectively across a wide temperature range, from surface values of 20 Celsius to upper level temperatures far below zero.

While some metals offer strength and resilience under both mechanical and thermal stresses, their electrical conductivity must also be considered. Often the goal of the mission is focused on storm electrification, therefore using conductive materials could interfere with data collection [3]. The final material choice must consider a balance of mechanical strength, thermal resilience, and electrical conductivity.

An intentional delay is incorporated into the system to distance the package from the balloon, preventing entanglements with local foliage or infrastructure. The letdown mechanism would benefit from being released as part of the balloon separating ensuring easier recovery of the instrument train. This topic is discussed further in Section 4.5.

Federal regulations must be followed to properly ensure that no further authorization is needed for any data acquisition flights. The regulation that most directly applies to this mechanism is 14 CFR 101.35(d) [4], which will be discussed further in Section 1.3. The letdown mechanism is just one part of a larger package and thus, minimizing the weight when possible is ideal. This guides the decision on some of the material choices of interest.

1.1.2 Failure Modes for Letdown Mechanism

The two primary shortcomings to remedy are preventing the line from having issues while releasing and ensuring repeatability of the parts. Consistency issues with previous field projects and test flights have shown simplification and ease of operation provide the best chance of securing quality data. Since the letdown is a vital part of ensuring data quality this mechanism carries high significance.

The redesign will help with the wear and tear of the system and make successive launches easier to set up in either a field or lab setting. An activation system is in place for the previous mechanisms and as such it can be manually operated; however, if an issue with the ground station arises, an onboard pressure based sensor will activate. The mechanism for operation used the nichrome wire to release tension on the bottom section of the spool thus allowing for a second attached line directly connect to the spool, allowing for distancing of the package.

1.1.2 Cutdown Mechanism

The cutdown portion of the project lies in the necessity for retrieval of the sensors after flight. Retrieval of the instrument train is one of the essential parts of data collection and, as such, this is a high priority task for the project. Dealing with upper level winds can make retrieving the instruments time consuming and resource intensive, emphasizing the need for an effective mechanism. Ending a data flight mission after the desired in situ environment had passed means the potential for a significant reduction in the distance required for retrieval. Figure 3 displays the previous mechanism which was attached to the main body of the cutdown/letdown mechanism.

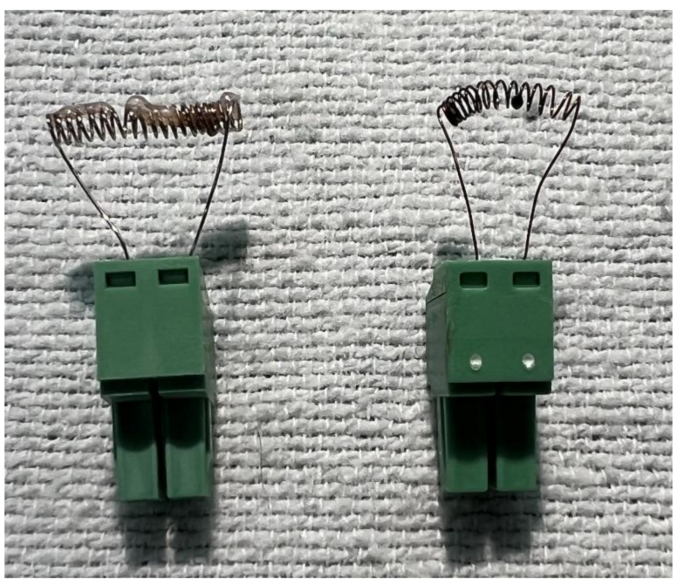

Figure 3: The Cutdown Mechanism for Flight Termination

The previous mechanism relied on the satellite control panel which was operated by a ground station and operator or an on board automatic sensor. This method ensures the person responsible for terminating the flight was in command of deciding at what point the instrument train should stop collecting data. The decision of when to end the flight will depend on the specific data objectives being pursued. In previous field campaigns such as the Lake Effect Electrification (LEE) field project, the flights most often ended after the balloon penetrated entirely through the shallow snow bands. This moment is determined by following the radiosonde data for relative humidity to determine cloud content.

Upon issuance of the cutdown command, a parachute which is part of the train of sensors and instruments, is then deployed through an immediate downward force pulling it into operation. Prior iterations of the cutdown mechanism have been activated in a very similar manner to the letdown mechanism.

The cutdown mechanism being triggered helps to prevent the balloon from traversing into regions where retrieval becomes much more difficult. These areas: oceans, remote mountains, and forests are avoided due to the effort taken to retrieve the sensors. Field projects most often have a geographical area for operations to be carried out. Previous launches have operated on a geo fence wherein the balloon might traverse outside that region, and an automatic signal would be sent triggering the cutdown and end of data acquisition.

While working in an intense operation period (IOP), it is crucial to be ready to launch again. Prior iterations of the cutdown mechanism were a single use and needed to be replaced after each launch. The nichrome wiring in Figure 3 needs proper spacing to work as it rapidly heats up and melts through the nylon line. This mechanism exhibits multiple recurring failure modes apart from this issue. In some launches, the mechanism would not heat enough, meaning that the line would stretch out and not release the package. Additionally, issues have been observed with improper wire spacing and the failure of the wiring to generate heat. In such cases, the release would only be due to the popping of the balloon.

1.2.1 Cutdown Constraints

There are several high importance constraints related to the cutdown mechanism within the scope of this project. The release mechanism is responsible for holding the instrument package under tension, it must reliably withstand both the static forces generated by the ascending balloon and the dynamic impulse forces caused by sudden jerks or oscillations in acceleration of the payload. If not properly accommodated, these forces could result in an early release or failure of the structural geometry, compromising the data acquisition mission. The forces tested and experienced in the system are analyzed in Chapter 2.

Another constraint is the repeatability of ease for resetting the mechanism for subsequent flights. Previous designs have proved challenging for rearming the mechanism due to field conditions and the need for precise calibration. The complexity present here limits the frequency of flights and delays data collection efforts. The new mechanism needs to be reliable but also robust and easily replaceable. An improved design that allows for reconfiguration will enhance operational efficiency.

1.2.2 Failure Modes for Cutdown Mechanism

The preceding method of cutdown had several prevalent issues regarding deployment and resetting. The time sequence for superheating the nichrome wire to melt the monofilament had caused problems. The coils need enough space between to fit the monofilament. If there is not enough space between the coils, any current will not properly circulate the wires. If the coils ended up touching, the high current would drop the battery voltage and end up turning the microcontroller off. This problem is identified only after recovery of the device had occurred.

The delicacy required to set up the coils is observed as an equally troublesome situation that can happen where the monofilament line moves around inside the coils and will thus have issues when triggered. The issues here are when in flight, the line fails to melt quickly enough and experiences stretching out and not experiencing a full release. This error method means inoperative failure, therefore allowing the balloon to reach the popping altitude. Figure 4 displays a burner that had been used in flight. The line is melted into the burn wire and and displays the one time use effect of this mechanism.

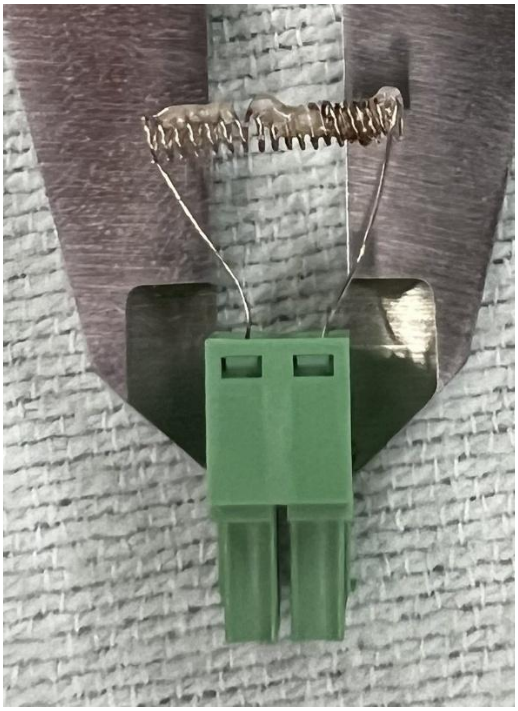

Figure 4: Failed Nichrome Burner

The burners are a one time use mechanism. As such, it is difficult and overall inefficient to continue with this mechanism compared to other methods. This part of the previous scheme is time consuming and less reproducible than a quick attachment method, leaving room for error in repeatability. The mixture of issues brought enough concern to redesign this system.

Finally, there is variation in the distance between the coils through human error and the struggle to accurately reproduce parts. Other methods of manufacturing parts remove human error or limit it to a point where it isn’t nearly as effective. This is worth noting as potentially the cause of many of the failures in the mechanism. As there is no current way to manufacture these burners aside from manually by hand, a new system is favorable.

1.2 Review of Previous Research and Efforts

This project is unique in that the current literature is sparse relating to prior iterations. Balloon launches with intended purposes go back to the 1940s when they were used for nuclear blast warnings [5]. The balloons were outfitted with aluminum foil for reflectivity on radar which could then be monitored. It wasn’t until the 1950s that a balloon featured a release mechanism. The MOBY DICK project was conducted by the United States Air Force whose main goal was to map upper level wind currents [5]. The system features a counterweight that could be manually triggered to allow the balloon to fly up. Upon finishing the mission, the balloon would cut down the package and a parachute would allow the instrument train to fall to the surface.

1.2.1 Ballooning at NSSL

Balloon launches have been happening around the country, but namely at NSSL since the late 1970s [6]. The idea of the electric field meter dates to as early as 1978 at Langmuir Laboratory for the exact study of thunderclouds [7]. Instrumentation used for applications of thunderstorm research has gone through various iterations over the decades. The Electric Field Meter (EFM) as well as the Particle Size, Image, and Velocity (PaSIV) probe [8], have been attached to study cloud microphysics. These platforms feature a fundamental issue with data retrieval.

The inability to actively transmit data from the PaSIV means that retrieval is a most essential part of the data collection process. For a time, retrieval meant waiting for the balloon to pop and manually searching around a rough area. The introduction of new technology such as mobile launch facilities [9] and spot trackers meant easier methods for finding the instrumentation and more versatile launching schemes.

Nichrome wire burners have been in use for many years. A project out of New Mexico Tech found the tightly spun wire to be efficient in cutting through the monofilament line [10]. By sending a large current of energy from the onboard 9 volt batteries to the nichrome wire, the burner becomes red hot and melts through the monofilament line. This method acts as the cutdown function to release at a predestined location. This mechanism was tried and tested over multiple decades of use. Issues began to arise in recent years with testing in field projects such as those discussed in the following section.

1.2.2 Cutdown Systems in Recent Use

Cutdown systems are essential for releasing the ascending balloon from the instrumentation package. This function is vital for preventing the balloon from drifting too far from the launch site and causing difficulties for the recovery process.

1.2.2.i Lake Effect Electrification Field Campaign

The LEE field project which took place in upstate New York in the winter of 2022 featured an updated version of this technology [11], [12]. Throughout several tests, it became apparent there were potential issues with the nichrome burner. Problems such as melting too slowly, the circuit not triggering properly and failing to send the current, and the premature release meant unsuccessful data acquisition flights. The repetition of various issues on this project led to interest in the modernization of the whole package.

1.2.2.ii Deep Convective Clouds and Chemistry Field Campaign

Deep Convective Clouds and Chemistry (DC3) fielded mobile ballooning equipment platforms for observing datasets on thunderstorms. Recording observations of the electrical structures as well as dynamics and physics, this field project used a similar cutdown/letdown method [13]. Operational data collected from this project spans collaborations with several educational institutions and government laboratories.

1.2.2.iii High Altitude Operational Return Unmanned System (HORUS)

The Global Monitoring Laboratory (GML) and Cooperative Institute for Research in Environmental Sciences (CIRES) launched a prototype high altitude air sampling instrument in 2021 [14]. This glider known as the High Altitude Operational Return Unmanned System (HORUS) used a high altitude balloon to reach 75,000ft (22,860m) where it began observations. This project sampled vertical air structure and featured a similar system to release the instrument package from the ascending balloon. This project differed from the traditional use of the cutdown mechanism as sampling began after release alternative to ending sampling at release.

1.2.3 Tensile Loads in this Project

Tensile loads such as the one present in the instrument train are subject to an impulse force once the line becomes taut. The nearly instantaneous force applied requires a given material to have some elastic characteristic [15]. This phenomenon was researched in a similar practice using mooring lines for ships to estimate the force at which a tensile line snaps. The model is similar to an ascending balloon where an applied force is pulling on an elastic line at which point the increased force is released.

To better model the testing data, a formula was introduced relating total force to partial force components. The formula in Equation 1 uses the $\vec{F}_{excit}$ as a placeholder for external forces moving on the vessel resulting in a force on the tensile line, $\vec{F}_{hyd}$ represents the hydrodynamic load induced by external fluid forces such as the wind and $\vec{P}_{re}$ represents the static tension on the line.

$$\vec{F} = \vec{F}_{excit} + \vec{F}_{hyd} + \vec{P}_{re} \qquad (1)$$

The relation between mooring lines and tension lines for this balloon project are similar in they are based on an applied load on an elastic line and the appropriate release of that tension.

The nylon monofilament line used in this testing experiences plastic deformation under tensile strain. This deformation creates weak points in the line where the material is strained to a new shape called necking, ultimately affecting its tensile strength [16]. The necking of this line shows it to be ductile. While the loading is primarily directional loading towards the package it is suspending, the tensile line exhibits equivalent deformation throughout the body until the load is released.

1.2.4 Relevant Issues with Simulations

Three dimensional geometries created in modern computer assisted design packages typically take the form of a homogeneous model. In SOLIDWORKS, when designing the parts for this project there are no voids or holes inside the geometry. This is done by simple extrusion. However, 3D printed parts are not entirely whole, and therefore the associated mechanical properties are not homogenous [16][17]. This finding is an important context for simulations run on any additively manufactured parts. For this research project this is not directly accounted for. However, the parts are manufactured to be as close to homogeneous as possible. This is discussed further in Section 3.5.

Ansys simulations rely on the computational capability of the finite element analysis. Mesh quality and element size are two factors that are influenced by the limitations of computational power. Mesh refinement is directly proportional to the accuracy of the study [18], [19]. The accuracy of these simulations is of high importance to understand the expected computed values carried out by the physical protypes. Furthermore, refinement of the mesh can resolve areas of high deformation and stress in the design where issues might arise.

The accuracy of solutions reaches a threshold where an increase in computational efforts yields diminishing returns. The values eventually converge to a point where there is limited variation for the increase computational power and time cost. There also exists a node/element limit in the student license of Ansys for refinement of a mesh.

1.3 Applicable Federal Guidelines

This project follows Federal guidelines strictly to ensure that any operations and mechanisms fall in line with the required specifications. Regulations controlling unmanned balloon launches are formally defined in 14 CFR Part 101 [21]. This part covers Federal guidelines for unmanned free balloons. This definition is what constitutes the official interpretation of data acquisition flights. All rules outlined in the CFR are strictly adhered to ensure proper care and safety of the public. There are a few specific regulations that are especially pertinent to this project which will be discussed.

Covering 14 CFR 101.1(a)(4), there are specific limitations on the weight of payloads. The weather balloon launch has two payloads: the mechanism package and the tethered instrumentation. Most often the EFM is the attached instrument. The rule states that if two or more packages are carried under the balloon, they must weigh under 5.44 kilograms (12 pounds) otherwise special authorization must be obtained before any flights take place [20].

The instrument train in its current configuration is under the weight specifications at 2 kilograms (4.40 pounds). This qualifies as one of the two allowable payloads. The other payload is the mechanism package at roughly 0.67 kilograms (1.47 pounds). This means both payloads fall under the weight constraint. This project puts a large focus on weight limitations to ensure the least amount of helium required for the launch is used as well as ease of launch for participants.

The other significant regulation is 14 CFR 101.1(a)(4)(iv). This regulation states that any device for suspension of the attached payload must be separated by an impact force of 50 pounds (22.7 kilograms) or less. Previously, this statute was not directly engineered as part of the design. This regulation highlights another key objective of the project: ensuring compliance with all applicable rules not previously followed. Reinforcing adherence across all aspects ensures consistency and accountability throughout any future launches.

1.4 Analytical Framework

The layout of this study uses a dual analysis approach wherever possible to enhance the reliability of the results. Each calculation or analysis method uses at least one additional method to ensure accuracy. The study begins with manual buoyancy calculations to establish foundational understanding of the forces exerted on the tensile line at different time intervals. Video analysis clarifies the exact moments when different packages become taut with the line, enabling more detailed assessment of force analysis. This method, mixed with manual calculation of applied forces, provides information on the jerk applied at different times on the tensile line.

Software is used extensively in this project from the development and assembly of models to the iteration of design and ultimate prototype. SOLIDWORKS and Ansys are essential tools used to optimize geometries that meet both application and environmental specific constraints. Analysis carried out through this software ensures designs are able to support the performance and safety standards for the balloon launches.

To validate the performance of individual models, physical and finite element analysis methods are employed. Each model is tested both in Ansys and physically to ensure the best results. This approach ensures a comprehensive understanding of the impact of different forces and how they influence the overall integrity of the manufactured parts. The interaction between the balloon and models are examined to record the response to dynamic loads throughout this project. These methods serve as critical tests for ensuring reliability.

Chapter 2. Characterization of the Balloon Ascent

2.1 Video Based Kinematic Analysis of Acceleration, Velocity and Position

Recorded videos of balloon launches were analyzed to visually assess the ascent of the train. These videos, captured by participants in the field, were shared in the project's official messaging group and downloaded for analysis. This method provides insight into the forces acting on the tensile line and the moments they occur at. While each launch environment contains unique characteristics, this approach works to establish a baseline for values such as the acceleration, velocity and force over time.

The moment the instrument train is completely off any surface, the buoyancy must overcome the nearly instantaneous downward force of the package. It is ideal to let the package float out of the hands of the crew launching the balloon to prevent any further downward force the balloon must overcome. In video analysis, an occurrence of downward motion was rarely observed once the package was released, given the proper release method.

The analysis begins at the determined time of free buoyancy of the balloon where it is no longer held within the launch tube [21]. This nearly instantaneous moment is captured in Figure 5. Upon release of the balloon from the launch tube there is an initial moment of free flight. This period is determined by the free moment of buoyancy during which the balloon is completely unrestrained until the moment the line becomes tensioned, and all segments of the instrument train are in ascent.

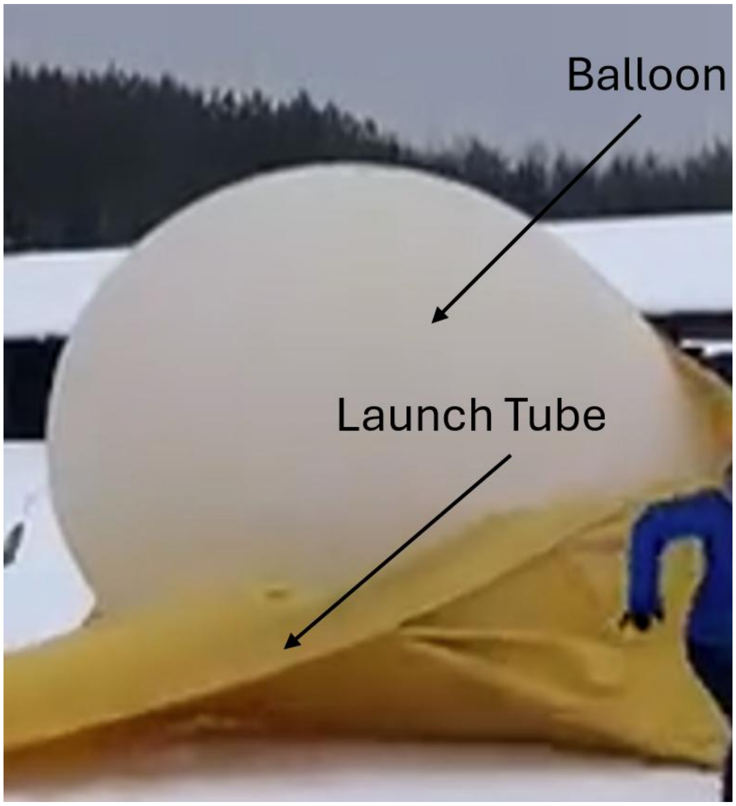

Figure 5: Balloon at Start of Launch Experiencing Free Buoyancy

This methodology employed using a stopwatch to pick out individual moments to be used for mathematical analysis. At the moment the balloon experiences free buoyancy, the stopwatch was started to determine the time taken to experience the first line becoming tensioned. This timing was performed manually to ensure an accurate reading of each step taken toward final free buoyancy in the balloon.

Human errors in the analysis must be taken into consideration, as they can impact on the accuracy and reliability of the results. To mitigate these errors, data of each individual flight was recorded five times to ensure overall consistency. The values were then averaged to produce a value more representative of the different time series for each individual flight.

The next step to record during a flight is the first package becoming taut. This moment and the subsequent moment of the second package becoming taut were then placed inside Microsoft Excel for analysis. Figure 6 displays the balloon and instrument train after both segments of line have become tensioned and the acceleration is constant.

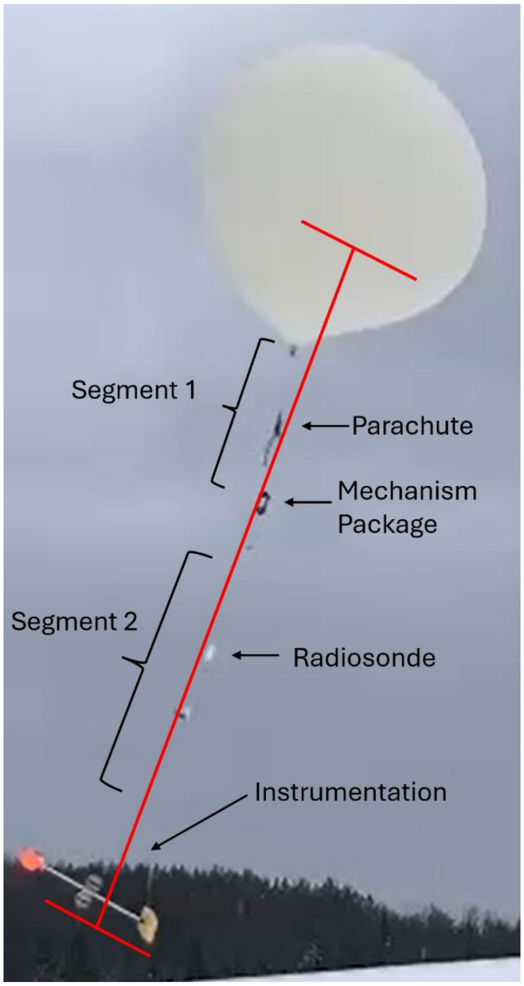

Figure 6: Balloon in Free Ascent with Aligned Axis

The range of time from when segment 1 becomes taut to the time segment 2 becomes taut depends on several factors. As previously mentioned, it is ideal to launch the balloon by allowing it to fly out of the hands to decrease the jerk exerted on the parts and lines. In one analyzed flight, there was a volatile release which caused the package to knock out of the hands of a participant, causing it to jerk the line slightly once it became taut. It was found that there is an average time of 0.59 seconds between segment 1 and segment 2 becoming taut and an average value of 1.14 seconds until the package is in free ascent again after the initial launch. All the values found in the visual analysis are shown in Table 1 below.

Table 1: Visual Analysis Results

Launch Number	1 N=5	2 N=5	3 N=5	4 N=5	5 N=5	6 N=5	7 N=5	8 N=5	Total Average
Segment 1	0.68	0.61	0.65	0.45	0.56	0.56	0.61	0.60	0.59
Segment 2	1.49	1.18	1.11	0.98	1.10	1.11	1.14	1.09	1.14

To further investigate, the five values then had a standard deviation performed to see the variability between each recorded number. The standard deviation of these values was under 5%. The variation in standard deviation values was in the order of 10 milliseconds or smaller, giving credibility to the results.

2.2 Buoyancy and Velocity Analysis

As an alternative to the video analysis, the buoyancy force of the balloon was calculated using a variation on Newton’s Second Law of Motion and Archimedes’ Principle. The total buoyancy force exerted on a balloon, B is calculated using the equation [22].

$$\mathrm{B} = \rho \cdot \mathrm{V} \cdot \mathrm{a} \tag{2}$$

In this equation, ρ is the density of the air displaced by the balloon, V denotes the volume of the air inside the balloons and a is the acceleration. This equation permits us to estimate the upward force on the balloon. Buoyancy here represents the “force” component of the Law, while the “mass” component $m = \rho \cdot V$ requires the necessary value for the volume and density. Using a value of 1.22 $^{\text{kg}}/_{m^3}$ at 273K for the density of air and an approximate volume of 12.8 m^3 for inside the balloon, this equation is solved for the buoyancy force *B.*

$$B = 1.22\,\frac{\text{kg}}{\text{m}^3} \cdot 12.8\text{m}^3 \cdot 9.81\,\frac{\text{m}}{\text{s}^2} \tag{2}$$

$$B = 153\ \frac{\text{kg} \cdot \text{m}}{\text{s}^2} = 153\ \text{N}$$

Using this buoyancy force, a free body diagram was developed to better visualize the different forces throughout the flight and launch cycle. This diagram is shown in Figure 7 where the total upward force is 153 N, and the corresponding downward forces result in 40.9 N. Using a free body diagram is beneficial for understanding what forces are expected in a static frame of reference at different intervals of the package. While there will be impulse forces at different time segments, static forces will be present throughout the entire time of the package.

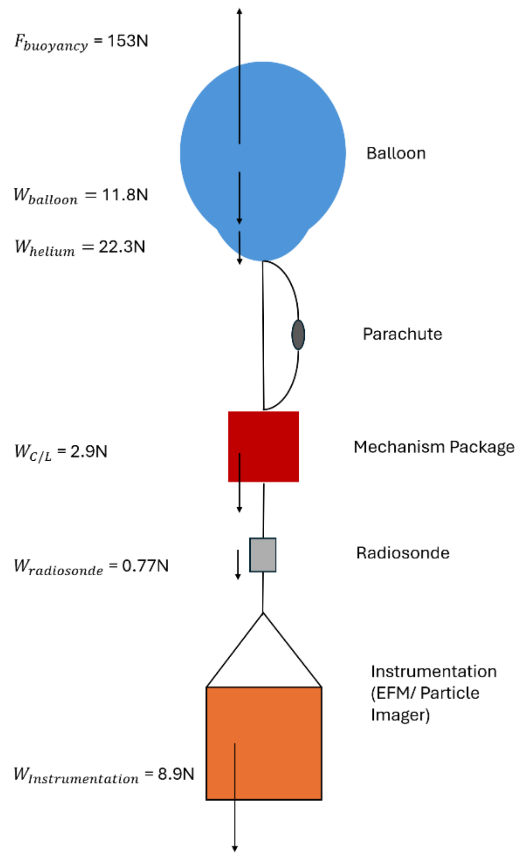

Figure 7: Free Body Diagram Showing Static Forces on a Balloon Flight

This figure gives a broader understanding of the different segments of the balloon flight and how the different static forces are experienced given standard temperature and pressure. Analysis in Section 2.3 gives some insight into how the impulse forces applied to the cutdown/letdown mechanism are experienced through the different stages of the buoyant package.

While the value of 153 N accounts for the maximum buoyancy experienced through the line, it is important to understand the difference between the maximum buoyancy i.e. the maximum upwards force and the net force experienced in the flight.

This relationship is understood further by subtracting the drag force and static force of the mass on the line. Equation 3 below displays this relationship.

$$F_{net} = m_{air} \cdot V \cdot g - m_{helium} \cdot g - F_d - F_{static} \quad (3)$$

In this equation, F_d represents the drag force on the line while F_{static} is the static downward force on the line. To calculate the drag force, Equation 4 was utilized.

$$F_d = \frac{1}{2} \cdot C_d \cdot A \cdot v^2 \quad (4)$$

To properly understand variations in velocity, data were averaged to determine an average velocity for the first minute of flight time. This flight data was recorded from a radiosonde and given in knots. The average value for velocity is 6.78 $^{m}/_{s}$. This value can be cross checked with theoretical calculations to determine the terminal velocity of an idealized balloon flight.

$$v = \sqrt{\frac{2[V(\rho_{air} - \rho_{helium}) - m_{total}] \cdot g}{C_d \cdot A \cdot \rho_{air}}} \quad (5)$$

This equation utilizes all forces on the line and ultimately accounts for the terminal calculated velocity. The resulting value of 6.80 $^{m}/_{s}$ gives context and reasonability for the value of 6.78 $^{m}/_{s}$ as previously discussed.

2.3 Analysis of Acceleration Variation

Analysis from both video and estimation from mathematical calculation shed some light on the forces on the instrument train. An equation was developed in order to understand how all the known values in the line affect acceleration. This equation uses the computed value of buoyancy from Section 2.2, static mass under the line, mass of helium and the drag force to quantify the net force in the line to then solve the acceleration. This calculation is performed by using Equation 6 as shown below.

$$a = \frac{(\mathrm{m}_{air} - \mathrm{m}_{helium} - \mathrm{m}_{package}) \cdot \mathrm{g} - \mathrm{F}_{d}}{\mathrm{m}_{\mathrm{system}}} \tag{6}$$

The calculation is performed to determine the net force which can then be derived to determine the maximum acceleration at the time segments. There is variation in the mass as the segments become taut, thus leading to changes in the value with respect to time. An empty balloon has an approximate mass of 1.2 kg, and helium has a density of 0.179 $^{\mathrm{kg}}/_{\mathrm{m}^3}$. These values paired with the volume approximation in Section 2.2 can be substituted into Equation 7 to solve for the total balloon mass.

$$\mathrm{m}_{\mathrm{balloon}} = (\rho_{\mathrm{Helium}} \cdot \mathrm{V}) + 1.2\ \mathrm{kg} \tag{7}$$

$$\mathrm{m}_{\mathrm{system}} = 3.44\mathrm{kg}$$

The inclusion for m_{system} in Equation 6 is the sum of all the masses present at that moment. These values were 3.44 kg at free buoyancy, 4.11 kg at segment 1 being taut, and 6.11 kg once the final segment became taut.

The equation resolves that during initial free buoyancy, the acceleration value is approximately 10.2 $^{\mathrm{m}}/_{\mathrm{s}^2}$. There is a time frame at which the balloon stays in free buoyancy. This time frame is about 0.55 seconds until the second segment of the package becomes taut at 1.14 seconds. The change in acceleration drops the value to 8.51 $^{\mathrm{m}}/_{\mathrm{s}^2}$. This value stays constant until the second segment becomes taut. This moment sees a change in acceleration down to 5.65 $^{\mathrm{m}}/_{\mathrm{s}^2}$, a significant drop since the initial value at free buoyancy.

Figure 8 displays the plot of data for the change in acceleration and velocity values in the given time sequence. The perforated lines are decided from average values calculated in Section 2.1.

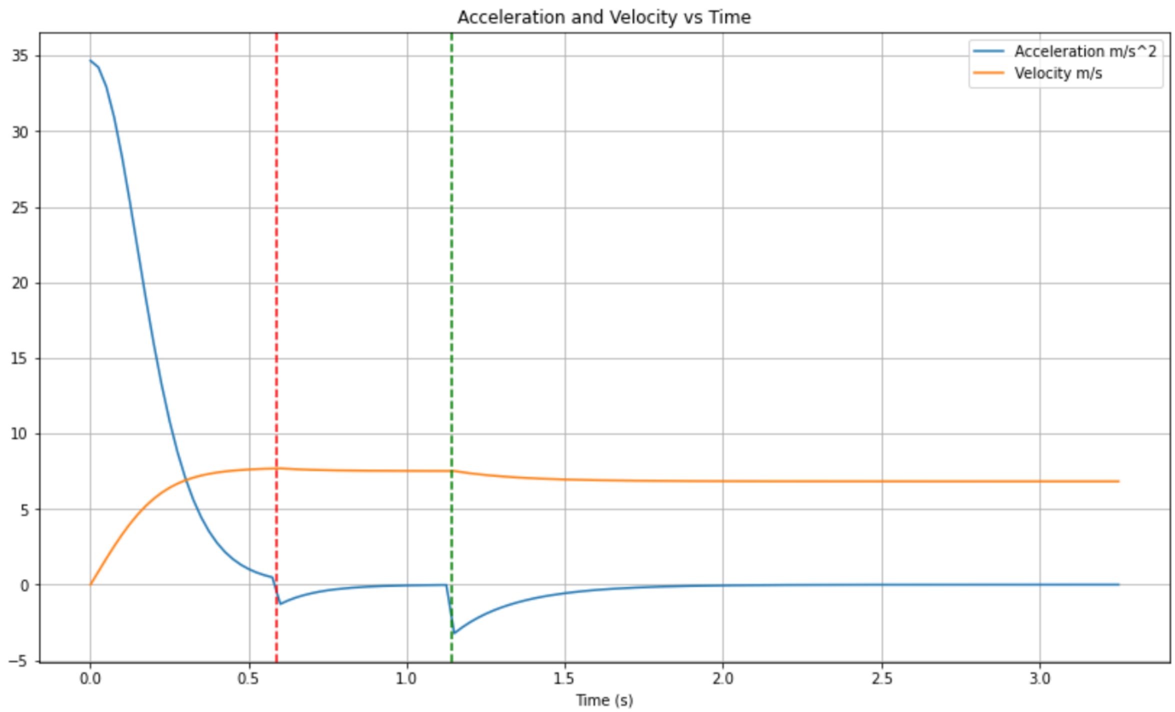

Figure 8: Acceleration and Velocity Plot

The calculated results show acceleration decrease with the corresponding masses becoming tensioned. This concept reinforces the understanding there are differing forces pulling on the line at different times. The acceleration dips below 0 several times as it recovers to an eventual steady constant value. The negative dips represent it slowing down due to these changes in mass. The corresponding changes in velocity help to identify the areas which terminal velocity are exhibited in the flight until it flattens out in the plot.

2.4 Estimate of Impulse Forces Exerted on Mechanical Components

Estimating the forces exerted on the line allows for cross reference of different values over time that the geometries must overcome. The average time values discovered in Section 2.1 account for the change in time between each acceleration value. To find the changing velocity values, the results from Section 2.3 can be used in Equation 8 below [23].

$$v_1 = v_0 + a_1 t_1 \tag{8}$$

Since the equation is accounting for an initial response, the v_0 value is zero for the first velocity. Segment 1 of the launch provides a value of 6.02 $^{m}/_{s}$. The value for the first segment velocity is important to solve for the second segment.

$$v_f = v_1 + a_2 t_2 \tag{9}$$

The second segment velocity is 10.7 $^{m}/_{s}$ using Equation 6 above. The time value used in Equation 9 is the difference between 1.14 and 0.59 to account for the time of the second acceleration value. The two velocities are important to solve for the impulse forces given each applied mass. To calculate the force, the impulse momentum equation [24] was used.

$$F_{impulse} = m * \Delta v \tag{10}$$

Equation 10 uses the two mass values discussed in Section 1.3 and applies them to find the force. The equation uses the Δv which comes from the difference between the final velocities for each time step. Δv for the first impulse is the difference between 6.02 and 0, while the second impulse is the difference between 10.7 and 6.02. Equation 10 reveals an impulse force of 4.03 N·s for the first segment becoming taut and 12.5 N·s for the second segment becoming taut. It is important to distinguish the difference between N and N·s, as newton on its own represents a force while newton second represents a unit of impulse.

These force values are the absolute maximum given the previously recorded launch procedures. It is also important to understand these values are not a persistent force but instead applied at a very short amount of time. The more often case has less impulse since the package is released lightly. In this circumstance, the force is more like the total static force of 40.9 N of the instrument train once everything has become taut.

Chapter 3. Modification of Cutdown Letdown Mechanism

3.1 Layout and Component Geometry

In this project, quick prototyping of parts became an essential effort. The process of quick and iterative prototyping was important for early renditions of the hook and latch mechanism. The inclusion of weight and size constraints meant that quick adjustments to the model were needed. The modeling for manufacturing and assembly of parts, was performed using SOLIDWORKS 2023.

The method used for the cutdown mechanism was initially a system of material removal such as burning or cutting. Prior versions used a nichrome wire burner as the main method for the release of the tensioned line. This process was effective but had many challenges associated with it such as failure to completely release or not efficient enough burning to melt entirely through the line. It became a focal point of this project to find a design that would not require a destructive element. To eliminate the need for these destructive release systems, a hook and latch mechanism was chosen. Figure 9 shows a SOLIDWORKS model of the mechanism. This chosen method is ideal as it creates ease of application by the simple mode of release being gravity and attached weight.

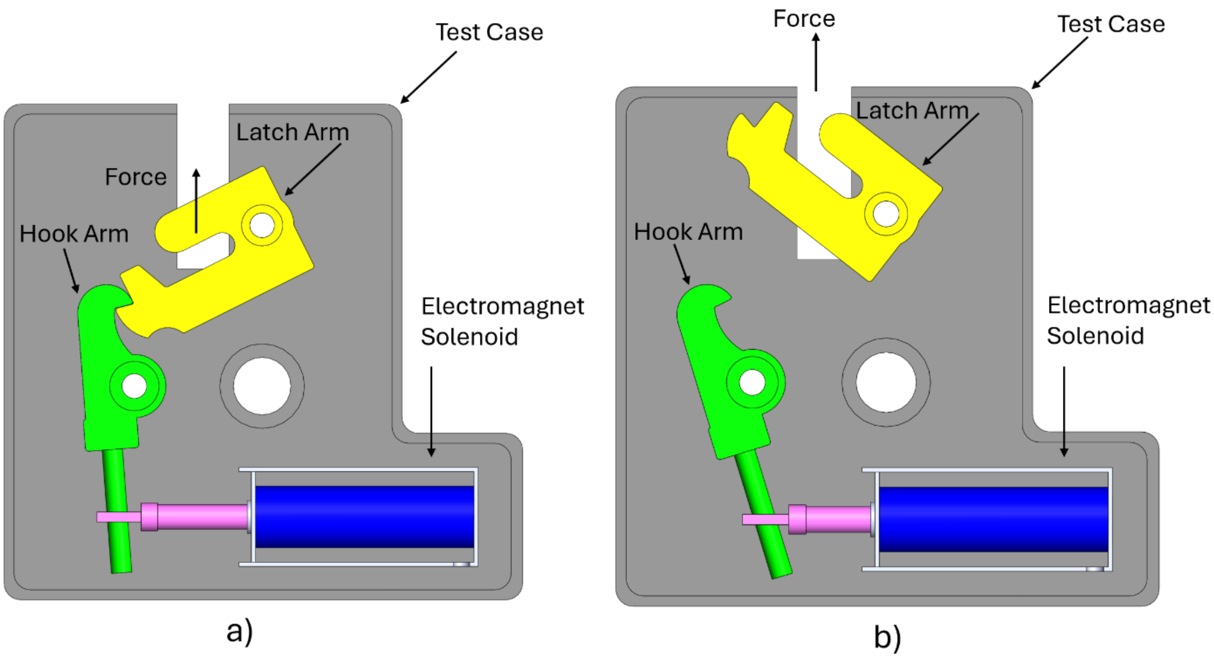

Figure 9: Cutdown Mechanism a) During Flight, and b) After Release

This system allows for a mechanical latch arm to be locked into place by an upward force of the hook arm. This force holds the latch arm in place while it has a tensile load exerted on it. The load from the balloon in conjunction with the hook arm keeps the latch arm stationary until the time when it is ready to release, at that point the electromagnet solenoid pulls the hook arm and releases the tensile force holding the latch arm in place.

The electromagnet solenoid placement is crucial to ensure proper retraction force capable of pulling the hook arm back. As previous mechanisms have used electrical components, the printed circuit board has connectors available for ease of application using this electronic component.

3.2 Proposed Latch Geometry

Iteration of design in this project was of the utmost importance in the continual evolution to a functioning design. The results from physical and simulation testing provided inputs to this process. This section will highlight each individual design tested of the four different designs and the changes in geometry between those parts. The findings from each Ansys revision are discussed in Section 3.6.

The practicality of the size of parts and limitations on weight incentivized a small but efficient manufactured geometry. This goal influenced the first test piece to be manufactured small thickness (2.50mm). While this might have been a causal reason for failure, there were many other issues found with design that required refinement. Figure 10 displays the first model tested during the project.

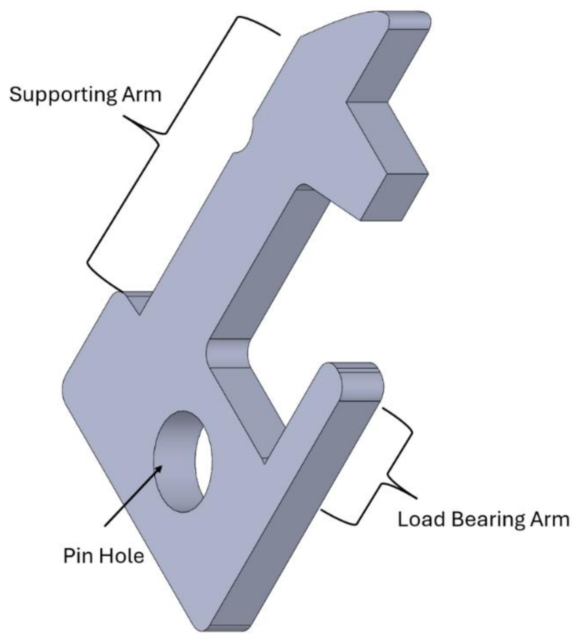

Figure 10: First Iterative Design

The load bearing arm had insufficient support and there was too much room for movement. This meant that as the package line became taut and then released some of that impulse force, it allowed the line to move around the interior and ultimately snap the load bearing arm. The following iterations of the design followed the idea of concentrating material where the forces were tested. The second latch model was then developed and subjected to Ansys simulations and drop testing.

Figure 11 displays the second iteration of the latch model for testing. The largest changes in the designs are featured in this figure to show the iteration process. This design features the most incremental transformation from the previous state.

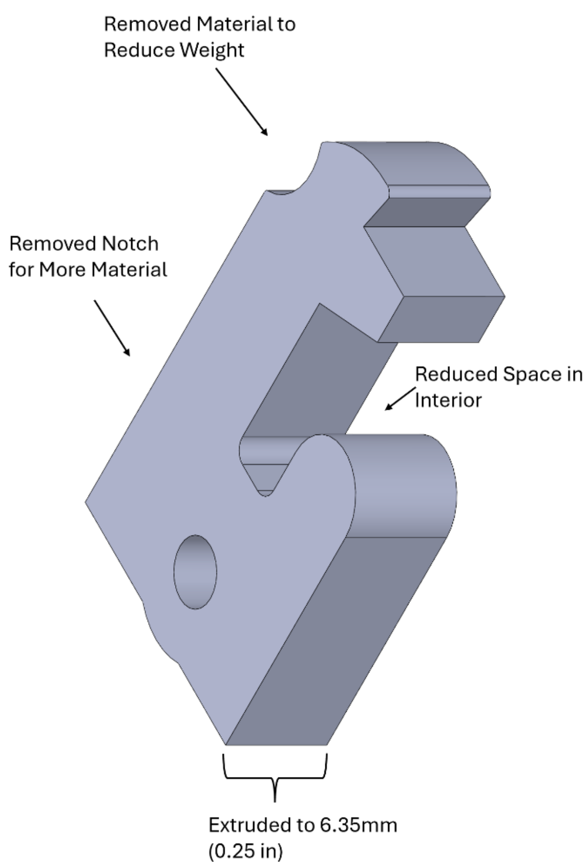

Figure 11: Second Iterative Design

The largest changes in this new model are reinforcement at the pivot point, reducing the size of the interior opening, rounding out sharp corners, and reinforcing the load bearing and supporting arms with more material. Reinforcement of the pivot point ensures greater resistance to the stress, ultimately reducing the failure under the testing. Rounding out the sharp corners is a large reduction in the stress as a deterrent against failure. The second design also features a notch taken out in the corner of the load bearing arm. This small change was made while testing fitting with the hook arm where at times there would be some rubbing against the geometries. This feature also slightly reduces the weight of the part.

Design three had the largest changes performed on the supporting material around the pin hole. The change in design in this step was focused on findings from Ansys where the deformed stressed region had yielding in the corner where there was insufficient material supporting the load. Figure 12 displays this new model with the increased support material adjacent to the cavity.

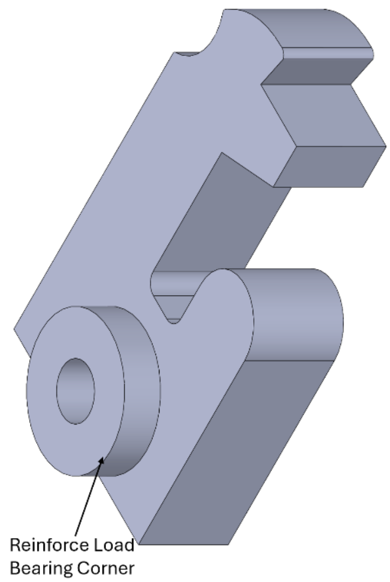

Figure 12: Third Iterative Design

In addition to reinforcing the material in the load bearing corner, the third iteration can distribute the applied stress more efficiently across the geometry. Incorporating support material is a crucial role for this by increasing the surface area over which the stress is applied.

The fourth iterative design features a slight difference from the third design. The main difference here is the amount of support material on the top side of the model. Reducing the overall radius of the support material allows for strengthening without the need for extra material. The second feature brought forth is to limit the amount of friction rubbing on the part and to allow for a torsion spring to be placed between the case and the latch arm. Lastly, the load bearing arm length was increased for greater success in testing. Figure 13 shows the fourth and final iterative design which is used in the prototype.

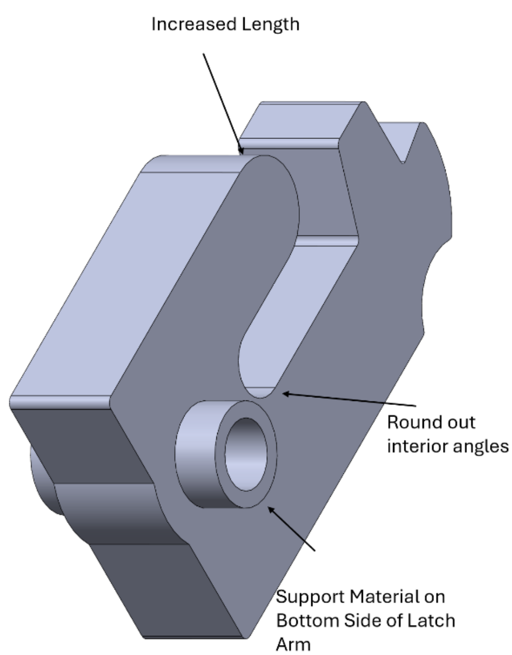

Figure 13: Fourth Iterative Design

The inclusion of support material on the bottom allows for a torsion spring to be placed under the part. This spring allows for easier assembly when putting the arm into position. The spring acts in torsion and keeps the latch arm forcing upwards, which is especially important when the monofilament line is not in tension prior to launch.

The fourth design also features an increased length of the load bearing arm. This is to combat vibration in the mechanism ultimately releasing the attached package. The increased length of this part also ensures that it takes a significant amount of movement to fully release and nearly removes the possibility of this entirely. The final geometry is the latch mechanism to be used in the physical prototype. Later sections will discuss the other factors considered for choosing this geometry.

3.3 Proposed Hook Geometry

The hook geometry is vital as it must be able to resist force of the latch arm pulling upwards. The hook at the top of the arm fits in place on the latch arm and locks the arms into place until the electromagnet pulls backwards on the pull pin releasing the tension of the part and ultimately releasing the attached package. Figure 14 displays the hook arm geometry. This design did not feature any significant changes through the iteration process. The only feature which was changed from the initial design is the supporting material on the bottom side and the rub plate where the two arms touch.

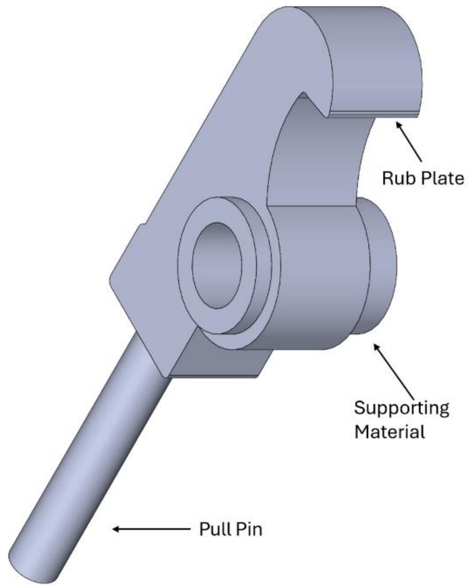

Figure 14: Geometry of Hook Arm

Ensuring the quality of this geometry is important in that this part links the mechanical and electrical aspects of the entire mechanism package. Failure in this part could signify failure of the entire launch sequence and data collection.

3.4 Proposed Manufacturing Material

Material selection is highly essential for this project to assure adequate structural performance. Polylactic Acid (PLA) is a strong candidate for manufacturing due to the low cost of filament, paired with biodegradability [25]. PLA is also considered a low skill filament with minimal limitations for manufacturing. Testing done by Özsoy et al 2021 proved a bending strength of 87 MPa on manufactured parts with a density of 1.24 $^{g}/_{cm^3}$. Many of the attractive features of PLA are due to the rigid molecular structure giving a higher stiffness but with low ductility. The high stiffness value is an interesting and attractive feature of this material, leading to testing being taken out on it.

Acrylonitrile Butadiene Styrene (ABS) is commonly considered alongside PLA when an experiment is done with one of these materials. Ductility is a great benefit of printing with ABS as tested prints resist breaking and often experience yielding before fracture. ABS has butadiene in it which exhibits rubber like properties providing resistance to impact [26], [27]. Manufacturing with this material provides great heat resistance while giving good strength and rigidity [28]. ABS struggles with low temperatures and humidity, leading to decreases in ductility [29]. The nature of this project means atmospheric temperature values are significantly below 0 degrees C and moisture is often very high in cloud level. Further, ABS is not biodegradable and has lasting effects on nature.

The final material tested is the Polycarbonate Carbon Fiber blend (PC CF). Polycarbonate is a lightweight but highly impact resistant material. As polycarbonate can be used in additive manufacturing, its high strength and lightweight nature make it an attractive choice for this application [30]. The high melting point for this material also ensures good temperature resistance (114 °C) in manufactured parts [31]. The inclusion of carbon fiber strands in this material provides greater strength values and higher wear resistance.

3.5 Additive Manufacturing of the Latch Arm

Rapid prototyping is a key concept of additive manufacturing of parts [32]. The ease of access using computer assisted design software means parts can be optimized to leverage material in the most stressed regions. The iterative design process meant that as failure occurred there would be a relatively easy process to modify and re manufacture for further testing. The increased ability to alter and modify the smallest changes within a design can represent the difference between the failure of a part and a successful test. The capacity to manufacture internally at The National Severe Storms Laboratory meant that the time between physical tests was minimized and tests could be carried out expeditiously.

Fused Deposition Modeling (FDM) manufacturing as done in this project is greatly reliant on the infill percentage [26], [33]. The goal of the latch arm model was to increase the stiffness and strength of the part while limiting deflection to prevent early activation of the release system. It was decided to use a 100% infill on all the parts to most closely resemble the homogeneous model presented in SOLIDWORKS as well as provide the most durability of the parts.

To optimize the strength and durability of parts, different printing orientations and infill patterns were reviewed. Concentric print pattern is the most efficient pattern for the load bearing properties exerted in this project. Due to the ability to orient the load transversely on the individual layers allows for the most significant shear strength. Figure 15 shows the concentric pattern which traces the model perimeter and makes it smaller as it moves inward toward the center of the model while Figure 16 shows the right arm mechanism using this pattern. This is an ideal format for the manufactured parts as it emphasizes directional lines on the load bearing arm.

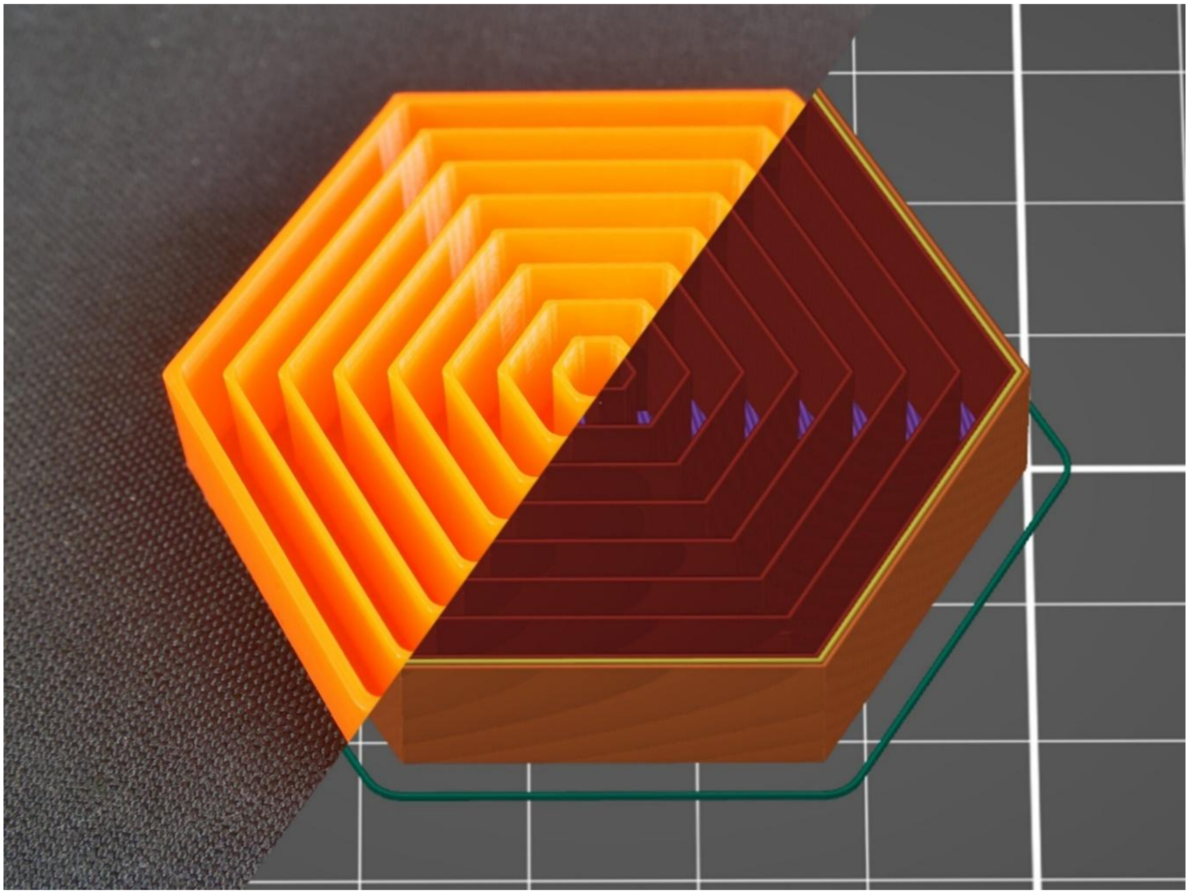

Figure 15: Concentric Fill Pattern Example [33]

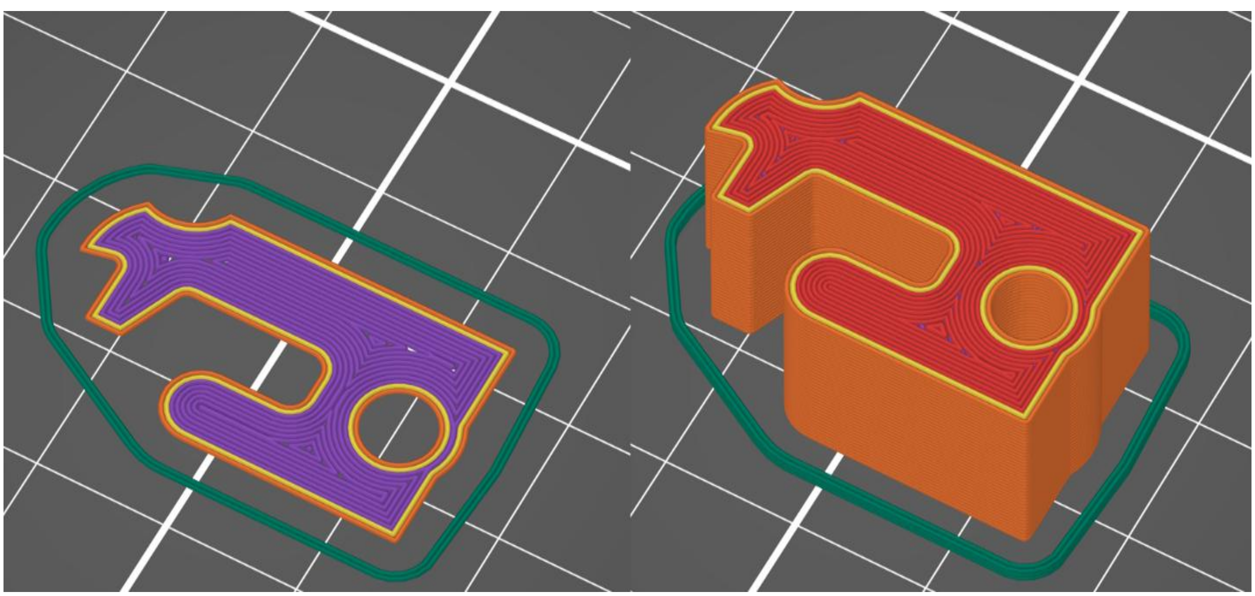

Figure 16: Latch Arm in a Concentric Pattern

Using the PrusaSlicer 2.8.1 software, these formats were manually selected and altered to ensure quality testing across several different variables including infill percentage. Determining the most effective infill percentage comes down to several factors for manufacturing. Infill directly relates to the amount of material and time spent on manufacturing parts and thus is a limiting factor when considering large models. This, however, was not of large concern for this project as the designs are small in nature (<1.5cm). Birosz et al. 2022 determined that increasing infill had a direct correlation with the force needed for deflection on a bending test [34].

3.6 Finite Element Analysis of Latch with Predicted Force Load

Product design is a critical factor in influencing the failure modes observed during development. Due to the dynamic environment this equipment experiences, the prototypes must stand up to all possible forces acting. The two most prevalent analyses in this project dealt with stress application on the load bearing arm of the latch mechanism and the associated deformation. The Ansys analysis system allows finite element analysis to be performed. The process involves importing prototype geometries and administering different boundary conditions to solve the desired deformation and stress values. All four finalized parts were analyzed through Ansys.

The process began by working on a design through SOLIDWORKS 2023. Upon competition of a prototype part, it would then be converted to a Parasolid file where it was then uploaded to the Ansys Workbench. Once the file was uploaded and Engineering Data were uploaded by manually inputting the information to the Ansys Mechanical.

The materials used in the simulations are not readily available within the Ansys engineering data bank. Manually inputting the material properties was carried out to ensure the most accurate information for success of the simulations. This process is done by inputting a new tab on the data tab and putting correct values in the sections needed for testing. Values for any materials tested were directly imported using technical data sheets from the manufacturer of the filament. These materials came from Prusament, the same manufacturer of the 3D printer. Materials tested and their associated material properties are displayed in Table 2 below.

Table 2: Materials Properties of ABS, PLA and PC CF [35],[36],[31],[37]

Material Name	Density (g/cm^3)	Young's Modulus (GPa)	Poisson's Ratio	Tensile Strength (MPa)
ABS	1.07	0.20	0.35	42.0
PLA	1.25	0.02	0.35	51.0
PC CF	1.22	2.40	0.32	76.0

The boundary conditions were set up for the latch to be set as to test the working prototype. There was a cylindrical support in the pin hole that held the latch mechanism into place. This was placed to simulate the bolt that bolds the mechanism in place. A fixed support was placed on the lip that connected with the hook mechanism. This boundary condition ensures that the parts should be locked into place and not allowed to move during actuation of the mechanism.

Lastly, a force of 153 N was placed in the corner of the latch arm where the load would be located. The value of 153 N was chosen as this represents the maximum buoyancy given standard conditions of the balloon. The value calculated in Section 2.4 for the max force at any given point is 54.8 N, a number lower than the simulated load. The next step was to set the mesh for the finite analysis. To ensure accurate results, a refined mesh was used. Once the geometry was in place and the preprocessing was finished, and the simulation solve process was ready to proceed.

The main values of interest in the finite element analysis are the safety factor values. Safety factor is a value given when taking the ratio of the material's ultimate strength and the equivalent stress. The strength value given from Table 2 is a tensile strength, Equation 11 below demonstrates the relationship to solve for safety factor.

$$SF = \frac{Tensile\ Strength}{Equivalent\ Stress} \tag{11}$$

This is an important metric as it accounts for variability in the material properties and assists in ensuring safety for a system to not fail. Typically, when discussing mechanical components, a good metric to follow is a value less than 1 signifies failure. To ensure geometry agreement and material testing, a value greater than 2.5 is determined to be a success for all simulated geometries.

3.6.1 Finite Element Analysis of the First Iterative Geometry

The first model had many shortcomings as discussed in Section 3.2. These shortcomings were analyzed also by the FEA as being an overall problematic geometry. Figure 17 displays the deformation in the first geometry. The Ansys models properly display which regions in the geometry are exhibiting the most values, and in this case, it shows the significant deformation on the load bearing arm.

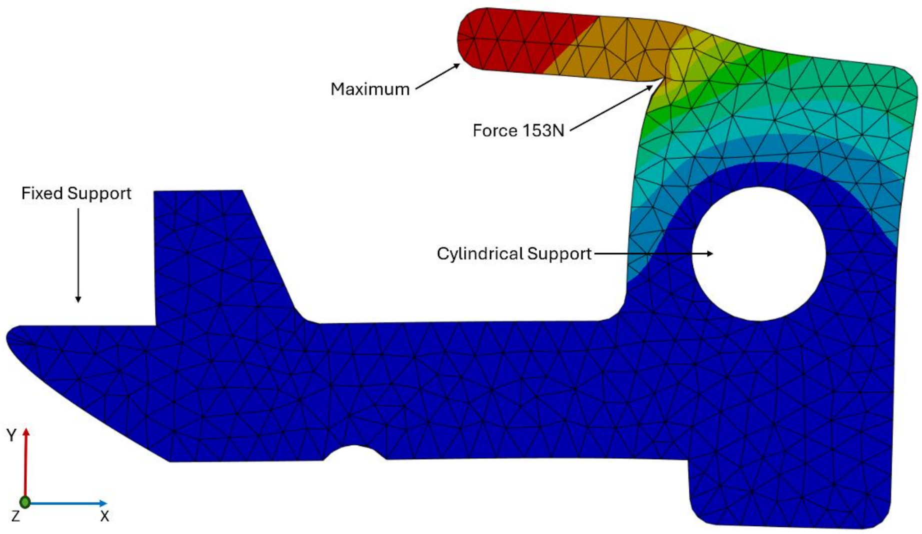

Figure 17: Total Deformation of the First Geometry

The deformation values across the three different materials tested left much to be desired. While no specific deformation metric is decided as leading to failure, the values for total deformation in the first geometry show significant movement in the load bearing arm, likely conducive to releasing the load.

The lack of material on the load bearing arm meant the stress focused most significantly in the corner where the force was applied. The maximum value of stress from Ansys is highlighted in Figure 18.

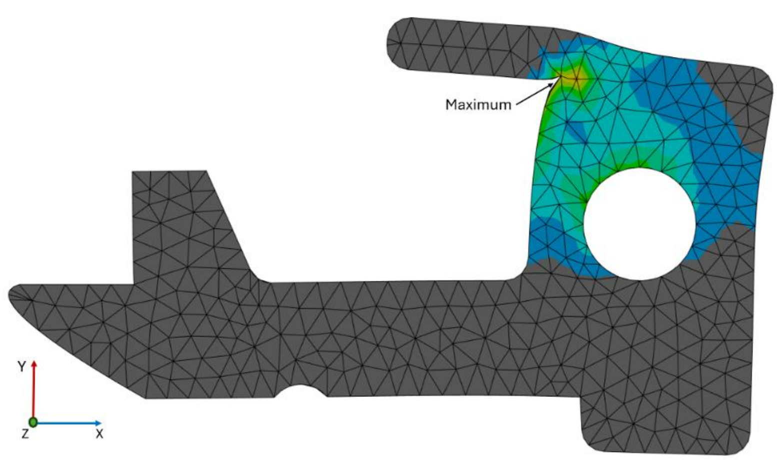

Figure 18: Equivalent Stress of the First Geometry

This model does an efficient job to show how the lack of rounding in the corner affects the overall stress in the body. The yellow contour displays the maximum stress. Table 3 below displays how the 3 different materials tested in this project performed on the first geometry. The values presented for the first iteration give insight to the failure of this part and the need to have a second iteration.

Table 3: Ansys Solutions for the First Geometry

Material	*Mesh Size (m)*	*Total Deformation (mm)*	*Vertical Deformation (mm)*	*Equivalent Stress (MPa)*	*Safety Factor*
PC CF	*8.72E-04*	*.24*	*0.18*	*122*	*0.627*
PLA	*8.72E-04*	*25.10*	*20.10*	*122*	*0.418*
ABS	*8.72E-04*	*2.88*	*2.31*	*122*	*0.344*

The total deformation and vertical deformation values show that PC CF was the most efficient for providing the least amount of deformation of the geometry. This value is of importance when considering the physical testing of parts. It is ideal for the lowest deformation values to ensure the part succeeds without fracture.

3.6.2 Finite Element Analysis of the Second Iterative Geometry

The second iterative geometry had a large change compared to the first design. The new features discussed in Section 3.2 provide better results when discussing deformation and stress. Figure 19 shows how the distribution of deformation across the model is recorded. This model provides great information on which areas are most likely to be affected by the force and to figure out ways to develop the design around those features.

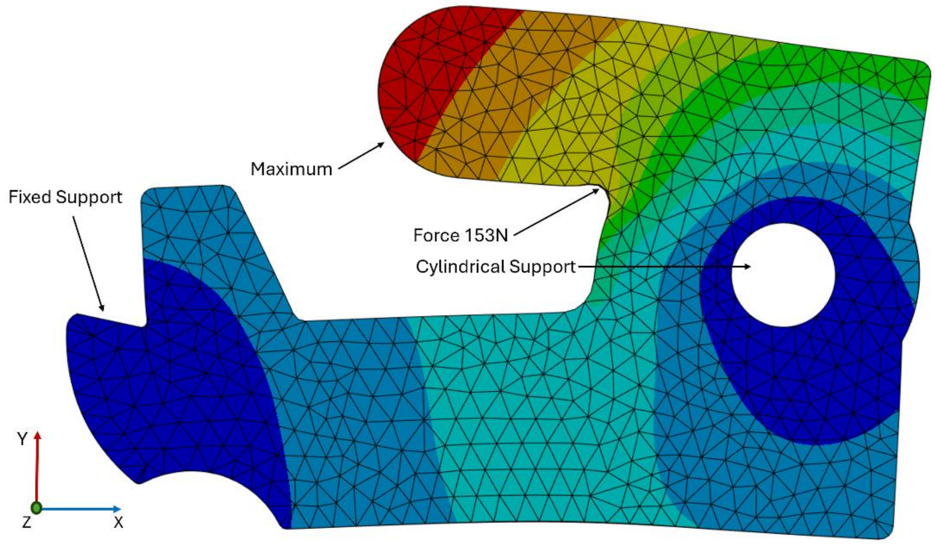

Figure 19: Total Deformation of the Second Geometry

The features discussed in Section 3.2 add increased support material near the corner where the load bearing arm is located, giving better distribution of equivalent stress throughout the arm and expanding deformation throughout the body. The equivalent stress distribution is shown in Figure 20 below.

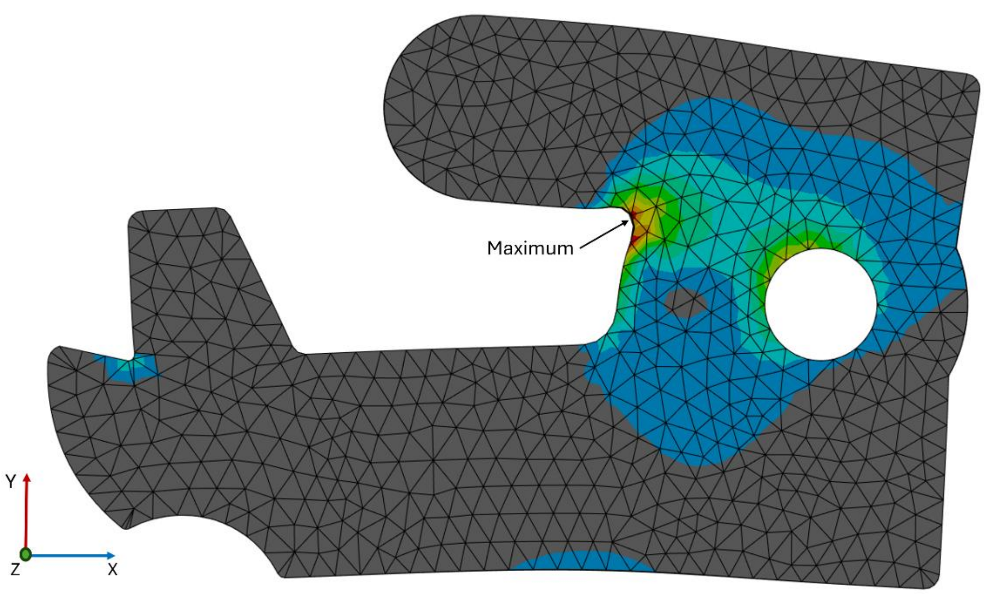

Figure 20: Equivalent Stress of the Second Geometry

The information from each Ansys solution allows for a greater iteration for further designs to be better suited for the needs. Comparing the results from the first iteration to the second iteration there is significant growth in the values. A notable feature is the spread of deformation and stress values throughout the body as opposed to the load bearing arm only.

The simulations on the second tested part yielded much more promising results than the first. The results in Table 4 show this growth in design directly because of more favorable values from Ansys.

Table 4: Ansys Solutions for the Second Geometry

Material	*Mesh Size (m)*	*Total Deformation (mm)*	*Vertical Deformation (mm)*	*Equivalent Stress (MPa)*	*Safety Factor*
PC CF	*8.72E-04*	*0.006*	*0.005*	*24.2*	*3.14*
PLA	*8.72E-04*	*6.870*	*6.120*	*24.2*	*2.10*
ABS	*8.72E-04*	*0.790*	*0.704*	*24.2*	*1.73*

There is a significant increase in values from the first geometry to the second geometry as displayed in Table 4. The max deformation of the load bearing arm is nearly one order of magnitude difference from the solutions in Table 3. The is important when relating to the physical testing carried out in Chapter 4. The increased material where the force is applied as well as supporting material around the pin hole are some features which helped produce these more favorable numbers. The safety factor from this set of tests increased significantly because of the geometric evolution. There is nearly a 400% increase in all values in safety factors from the first geometry to the second geometry, which is a good result.

3.6.3 Finite Element Analysis of the Third Iterative Geometry

The third design in this set of simulations brought the large supporting material upon the face of the latch arm geometry. Figure 21 shows an interesting characteristic on the load bearing arm given the force applied in the corner.

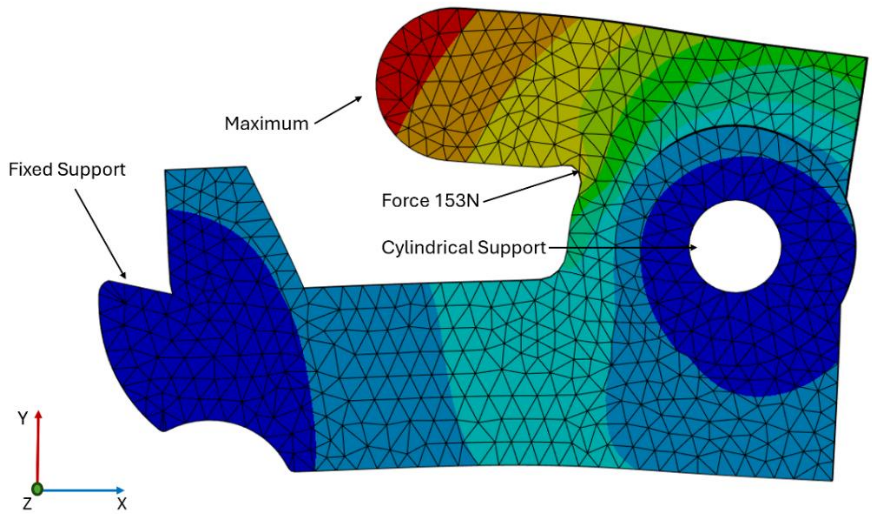

Figure 21: Total Deformation of the Third Geometry (Top View)

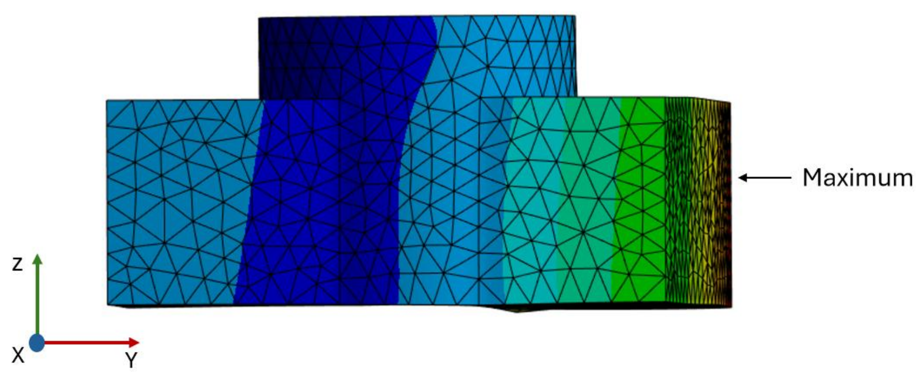

Figure 22: Total Deformation of the Third Geometry (Side View)

Comparing Figures 21 and 22, there is some upward rotation on each side of this upward extrusion of material. This feature is discussed as problematic in Section 3.2 for other reasons, but this finding in Ansys helps to shed some light on another issue. Later iterations of the latch arm featured lower upward motion due to decrease in the amount of support material.

The inclusion of supporting material is beneficial in further spreading stress values throughout the body. Figure 23 displays the equivalent stress for the third design. The figure shows how the force is applied in the same location, but at lower values. This supporting material is useful for creating a buffer between the point load and the remaining parts of the body.

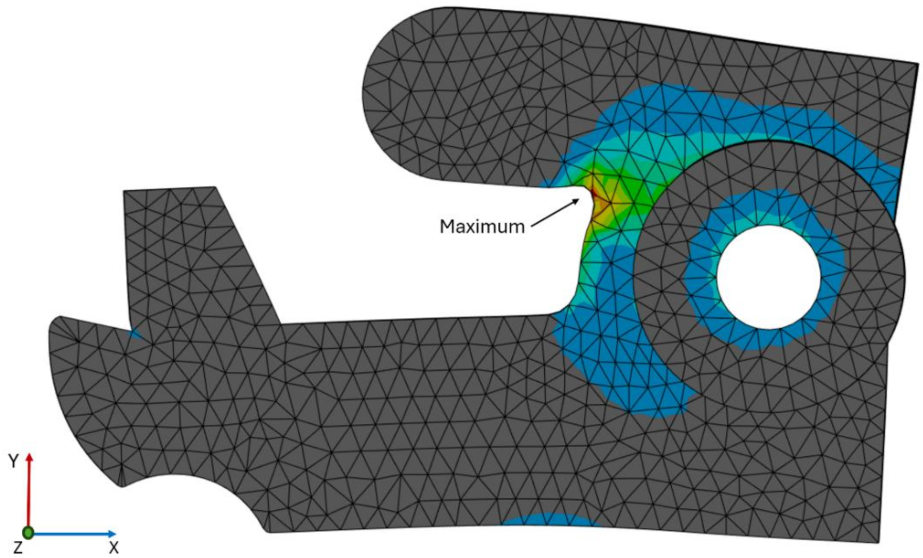

Figure 23: Equivalent Stress of the Third Geometry

These simulations produced an impressive set of data that is featured in Table 5 below. The information displays more growth towards lower values for deformation, higher safety factors and less maximum stress. This growth of values helps to prove the iterative design process as efficient.

Table 5: Ansys Solutions for the Third Geometry

Material	*Mesh Size (m)*	*Total Deformation (mm)*	*Vertical Deformation (mm)*	*Equivalent Stress (MPa)*	*Safety Factor*
PC CF	*8.72E-04*	*0.005*	*0.005*	*23.8*	*3.12*
PLA	*8.72E-04*	*6.170*	*5.430*	*23.8*	*2.14*
ABS	*8.72E-04*	*0.710*	*0.625*	*23.8*	*1.77*

The findings from the third set of simulations proved growth both in the design, and decreasing in the total deformation, vertical deformation, equivalent stress and the maximum shear stress. The decrease of all stress values supports the change in geometry, proving the worth of the supporting material.

3.6.4 Finite Element Analysis of the Fourth Iterative Geometry

The fourth iterative design worked to resolve rough corners and even out supporting material. This effort proved to be beneficial for the simulations. Figure 24 below shows the total deformation values across the fourth geometry. The feature to note is the dispersion of forces throughout the body and the influence of the raised support material around the pin hole.

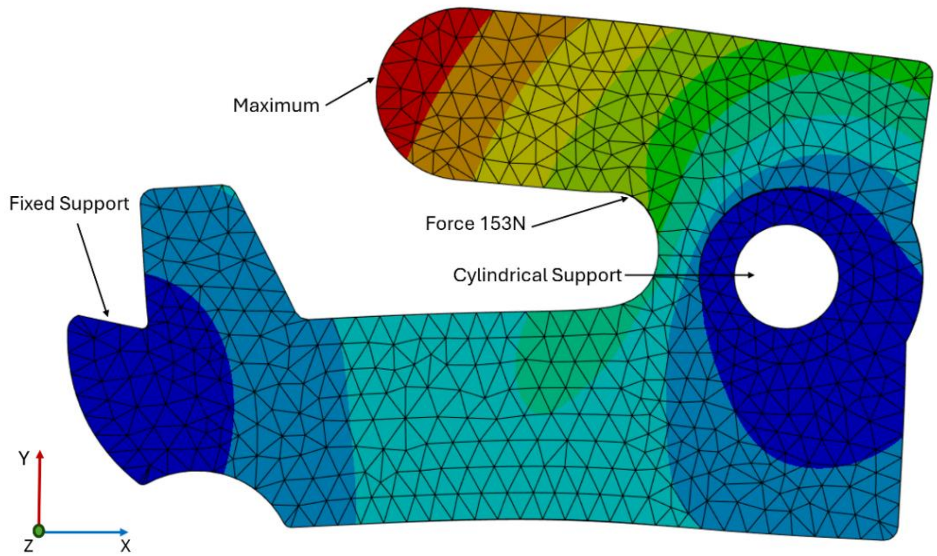

Figure 24: Total Deformation of the Fourth Geometry

The comparatively small deformation numbers prove this iteration the most effective geometry. The inclusion of support material on the top and bottom assists with stress dispersion around the body. Figure 25 shows this final iterative geometry and how the material assists with the applied force.

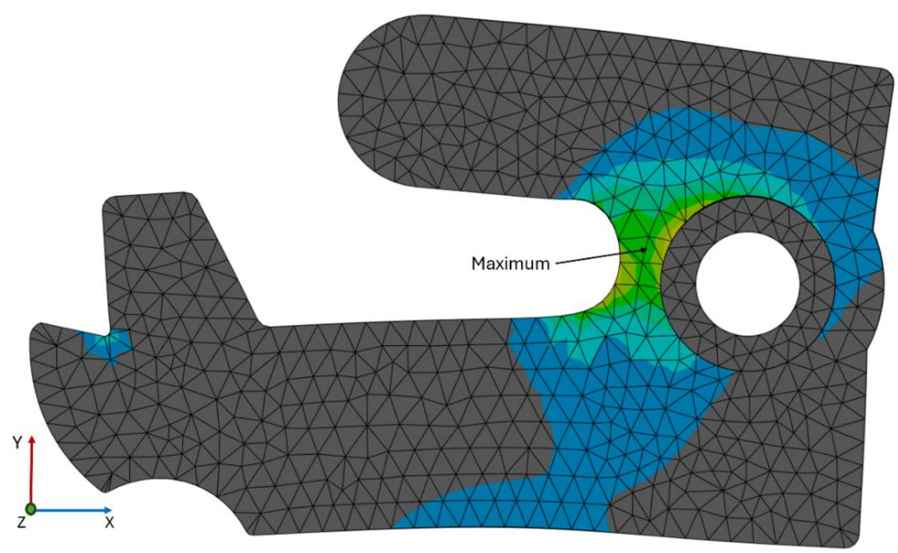

Figure 25: Equivalent Stress for the Fourth Geometry

This figure shows how the thinner support material had no stress values of note at the top section of the supporting material and reduces the amount of stress in the direct corner where the load is applied. This geometry is the final iteration for prototype testing.

The final iteration of the latch arm proved to yield the most promising results. The inclusion of a longer load bearing arm, along with the extrusion material on both sides of the pin hole gives this model the smallest maximum total and directional deformation values yet. The results in Table 6 also prove a large growth for safety factor as compared across all the different tests. The safety factor for all materials tested in this design are successful and over the 2.5 value threshold.

Table 6: Ansys Solutions for the Fourth Geometry

Material	*Mesh Size (m)*	*Total Deformation (mm)*	*Vertical Deformation (mm)*	*Equivalent Stress (MPa)*	*Safety Factor*
PC CF	*8.72E-04*	*0.040*	*0.003*	*12.9*	*5.91*
PLA	*8.72E-04*	*3.920*	*3.600*	*12.9*	*3.97*
ABS	*8.72E-04*	*0.045*	*0.041*	*12.9*	*3.27*

These results displayed the iterative process worked successfully. The finite element analysis ran through Ansys mixed with the physical force testing in discussed in Chapter 4 proved the model to be sufficient given the loads.

Chapter 4: Prototype Evaluation

4.1 Interpretation of 14 CFR 101.1(a)(4)(iv)

Subparagraph IV brings in an element to the launches that must be properly coordinated to ensure success at launch as well as align with Federal regulations. In previous flights, the nylon monofilament line used had an impact rating of 978 N (220 pounds). While there are different types of lines used in the instrument train, they all exceed the limitation. Since these values are outside regulations, it is imperative to ensure that all parts of the launch align with the rules.

The new challenge of ensuring the line would not snap at launch, but was strong enough to carry out the remainder of the mission lies in a shear pin. The ideal nature of designing a part for fracture given a specification is the variation in strength. The development of a manufactured polymer part is intentionally designed to break at a 50 pound (222 N) impact shear force. This inclusion allows for a small piece to ensure regulations are followed and that a simple modification can be made. The testing of a shear pin was carried out through similar methods to the manufactured arms. While similar extensiveness was not tested, the margin of error and time relative relation, any unexpected factor that might cause failure would have an instant release at the ground.

The option of using a similar method of implementing a 50 pound (222 N) line brings into discussion the error given by safety standards. Many options for line would have the lower limit of strength be at that factor and likely have much more strength given their intended purpose is not to break.

Utilizing Equation 12 the relation between the surface area of material and the maximum shear stress of PLA. The material choice of this section was chosen through similar means of the mechanism parts, but ensuring ease of manufacturing PLA was the final material.

$$F_{max} = \tau \cdot A \quad (12)$$

Given F_{max} must be 50 pound force and PLA has a shear range of 290-870 psi reliant on orientation, infill, and density it is ideal to be tested with the highest values as this ensures the least surface area for the shear pin ensuring weight limiting. Assuming the low end shear strength, value of 510, the diameter of the pin should be around 9.5 mm (0.375 in). Modeling and testing of these specifications took place. Figure 26 shows the design of the shear pin in SOLIDWORKS.

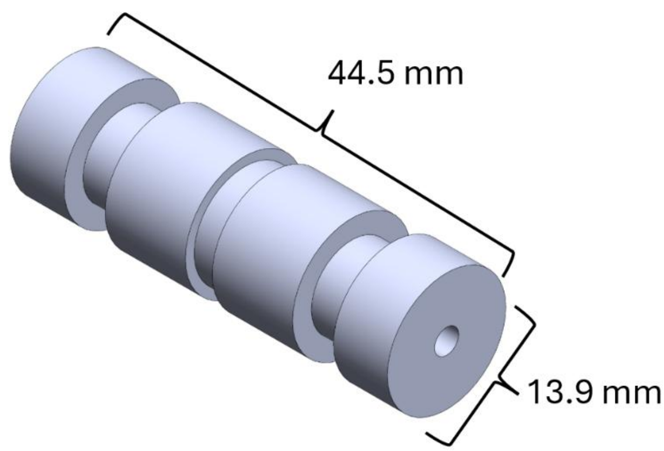

Figure 26: Shear Pin Model

This geometry was carefully designed to work most efficiently during the launch sequence due to the impulse forces present at this time. This geometry can be compared to Figure 27 where the part is manufactured. Figure 27 shows the shear pin with an untested part and a successful test result. The successful test part broke at roughly 210 N.

Figure 27: Intact Shear Pin and Fractured Shear Pin

4.2 Prototype Mechanism Package for Drop Testing

The mechanism package ready for drop testing is shown in Figure 26. This mechanism and the appropriate information regarding drop testing are discussed in this section. The system was set up to simulate different impulse forces given a mass being released at different heights to simulate the impulse force on the part.

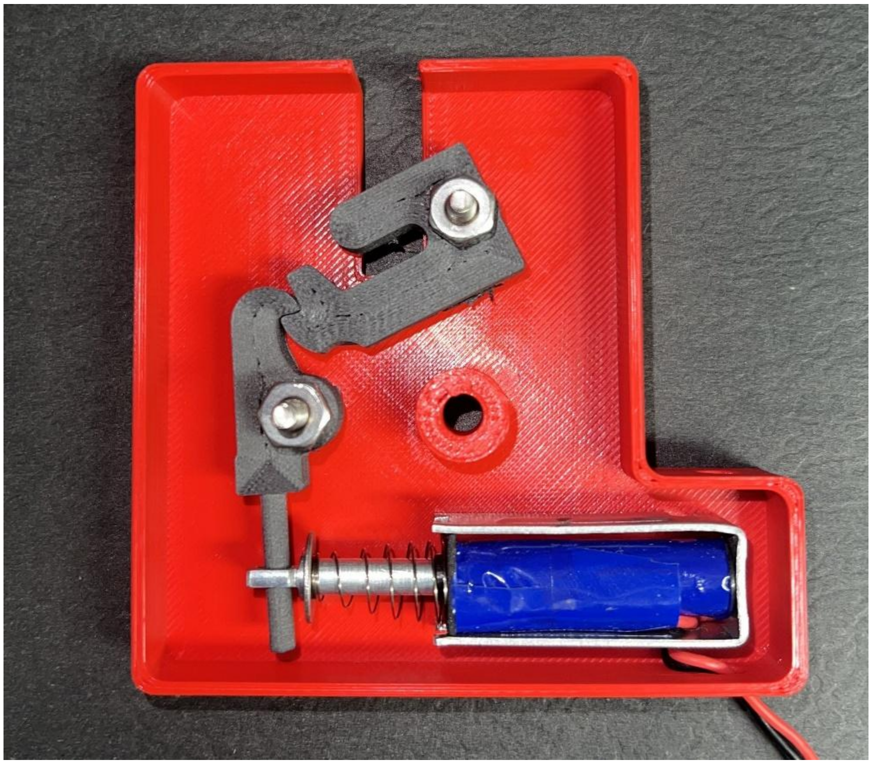

Figure 28: Prototype Mechanism for Drop Testing

The mechanism in Figure 28 is not the final proposed design. This package is purely for the physical testing stage. The final prototype, discussed in Section 4.5 features the assembly of the proposed design in alignment with the previous hardware.

4.3 Drop Testing in Lab

Simulations provide insight into idealized engineering tests, offering a controlled environment able to model the expected performance of models. Real world conditions introduce variability and often unpredictable factors that cannot always be accounted for. As part of the dual test approach, and to ensure reliability of these parts under operational stresses, extensive physical testing was conducted. These tests are vital to validation and viewing the performance of the manufactured parts.

A dedicated rig was employed allowing for repeatable force test application. The outcome of these tests was aimed at evaluating direct application of loads and the corresponding material integrity assessments. Subjecting these components to conditions often present in accurate test launch procedures can address potential failure points, allowing for the iterative design process to smooth these issues out.

One of the primary methods of force testing utilized the overhead crane present in the vehicle bay at the National Weather Center. This model was effective as it provided a fixed end constraint for the test rig, reducing errors caused by movement in the tensile line. The module demonstrated in Figure 29 was closely designed to provide the most applicable conditions present to those in a launch environment.

the simulations.

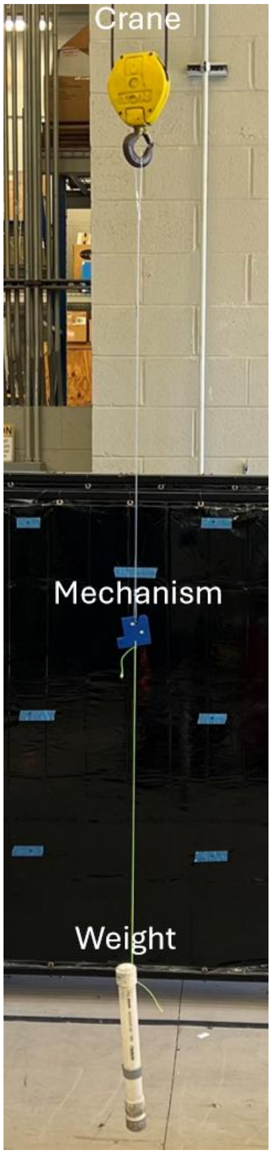

Figure 29: Physical Testing Rig

The results of force testing proved to be an invaluable step in the production and test process, allowing physical stress to be experienced by the components. Directly applying loads and solving the forces using Equation 10 allows for a better understanding of the response under tension and dynamic conditions present in this environment. The direct force testing confirmed the theoretical calculations presented in the simulations.

A test mass of 2.75 kg (6.06 pounds) was used to simulate the drop force associated with the package. The mass was dropped from a height of 3.5 m to keep consistency between tests and provide enough time for momentum to play a factor. To properly determine the velocity, Torricelli's Law [38] was implemented as displayed in Equation 13.

$$v^2 = u^2 + 2ah \tag{13}$$

$$v^2 = 0 + 2(9.81)(3.5)$$

$$v = \sqrt{39.24} = 8.30\, {}^{m}/_{s}$$

This equation yields a value that can then be used in Equation 10 to solve the impulse force. This equation results in a value of 22.9 N·s or 63.1 N given an approximate 0.36 second fall time solved by the value for velocity and height. The understanding here is that the momentum of a drop test is equal to that of a vertical tug exerted by an upwards force. In the case of this project, the buoyancy is the upwards force here.

The physical testing yielded binary results. This method was very beneficial for testing the impulse force exerted on the parts and if they were able to withstand a near instantaneous load value. The part either withstood the load applied and was labeled a success or fractured and was considered a failure. To stay consistent with the possibility of error in testing, five individual parts were tested at each level to decide the overall result for the part. If there was a single fracture result, the test would be labeled a failure. This standard yields a binary result of failure or success given the limited testing of 5 tests per part/material. The results from drop testing are displayed in Table 7 below.

Table 7: Drop Test Results

Material	First Design N=5	Second Design N=5	Third Design N=5	Fourth Design N=5
PC CF	Failure Five fractures	Failure One fracture	Success Zero fractures	Success Zero fractures
PLA	Failure Five fractures	Failure Four fractures	Failure Two fractures	Failure One fracture
ABS	Failure Five fractures	Failure Four fractures	Failure Three fractures	Failure One fracture

The PC CF proved both analytically and physically that it is the most efficient material. Compared with the fourth design proving the most successful for physical testing, the fourth design should be manufactured out of PC CF to yield the best results for use in the mechanism.

To ensure the parts were able to withstand a static force similar to the maximum buoyancy of the package, parts were set on the testing rig and hung with a static mass of 16.2 kg (35.9 pounds). There was no failure on any of the fourth geometry regardless of material.

4.4 Reverse Engineered Letdown Mechanism

To allow for ease of manufacturing of all parts, efforts were taken to design, modify and test new letdown spools. The result of this yields a very similar part as shown in Figure 2. The new design model, shown in Figure 30, shows similarities to the previous design.

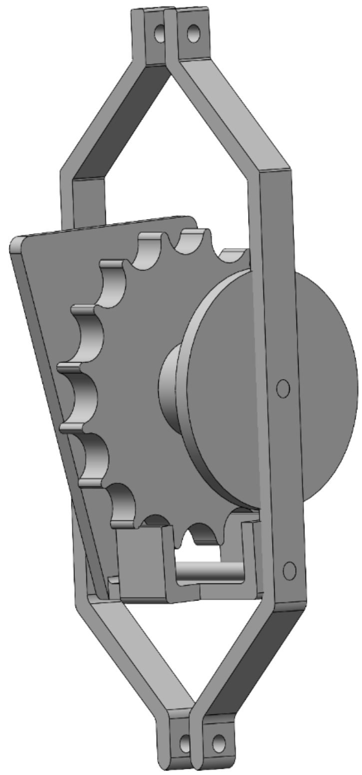

Figure 30: Reverse Engineered Spool

The spool has thicker features than the model in Figure 2. This is due to the polymers used to manufacture the part needing more substantial bodies to properly function. This model features the same main components however and manufacturing of parts is as simple as the cutdown mechanism.

A change to the order of mechanisms proposed an interesting though to the concern of dealing with tangled lines in trees. The proposed final design suggests the letdown spool be located above the release mechanism. This process then allows for the instrument train to still distance 30.4 meters from the balloon, while also removing the issue of tangling. Releasing the letdown mechanism improves the ease of operations and field recovery.

4.5 Final Proposed Design

Incorporating all design iterations, refined models and ensuring strict compliance with Federal guidelines has led to the development of the final proposed design. Various adjustments discussed in previous chapters have gone into this design to improve the functionality, durability and ease of integration within the overall system. Figure 31 presents the proposed designs and illustrates how they align within the larger system. The side plate fits properly into the mechanism package and will operate with the same overall tubular casing as before.

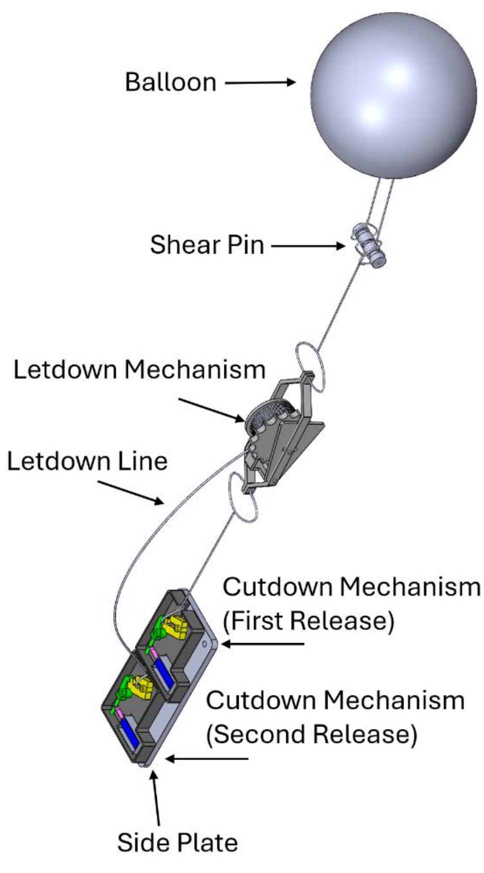

Figure 31: Proposed Design for Mobile Launches

The section of the system between the letdown mechanism and shear pin represents where the line will experience controlled separation during deployment. This region ensures the proper functionality of release while maintaining structural integrity under all applicable loads. For ease of visualization, Figure 31 displays this segment as a closed loop, providing a clear representation of its intended alignment within the system.

Due to the change in order, it is worth noting there will be two release mechanisms. One mechanism is for activation of the letdown mechanism, while the second is for the releasing of the package from the balloon. The first mechanism will hold on to the spool, keeping the letdown mechanism in tension and unable to begin distancing itself from the mechanism package holding all the components. The second release mechanism will be looped into the spool. This setup prevents the entire balloon from being released prematurely. The new method ensures that the second mechanism is holding on to the line until the data acquisition mission is finished.

Chapter 5: Concluding Remarks and Future Work

While the primary objective of this project was to design and manufacture a new mechanism for mobile balloon launches, an important aspect of the process involved integrating the updated components into the existing system. One key area requiring modification was the alignment of electrical systems in the previous housing. The most updated circuit board has been optimized for controlling the nichrome burners; however an adjustment will need to be made for the new electromagnetic solenoids to function properly even though it is not directly part of this study.

The proposed mechanism fits in place with the mechanism package tube as mentioned in Section 4.5. The available side plates are optimized for modularity and therefore placing the new mechanism and enclosure into place will be of little effort. Some minor geometry edits might need to take place to ensure there is enough space for the monofilament line to leave the overall housing, but this modification will be minor.

It should be noted, no physical testing with a balloon was performed. Theoretical calculations and mass based testing were able to estimate the expected forces, however, a full scale experiment would be beneficial to validate the values and test parameters. To address this interest, a digital force scale is currently being developed at NSSL to supplement the findings of this project. Future testing will involve fully inflating a 1.2 kg balloon and using the scale in line to properly measure forces in realistic launch conditions. Understanding the true magnitude of buoyant forces through a comprehensive physical test will provide insight into launch dynamics and the overall contributing variables.

References:

[1] Faber, J., Gerding, M., Schneider, A., Dörnbrack, A., Wilms, H., Wagner, J., and Lübken, F. J.: Evaluation of wake influence on high resolution balloon sonde measurements, Atmos. Meas. Tech., 12, 4191–4210, https://doi.org/10.5194/amt 12 4191 2019, 2019.

[2] Mokhov, I.I. and Akperov, M.G. (2006) Tropospheric Lapse Rate and Its Relations to Surface Temperature from Reanalysis Data. Atmospheric and Oceanic Physics, 42, 430 438. https://doi.org/10.1134/S0001433806040037

[3] Chester, G.V. and Thellung, A. (1959) Proceedings of the Physical Society, 73, 745 766.

[4] U.S. Federal Aviation Administration. 14 CFR 101.35(d) – Operations of Airborne Lighter than Air Craft. Electronic Code of Federal Regulations, U.S. Government, https://www.ecfr.gov/current/title 14/chapter I/subchapter F/part 101/section 101.35.

[5] Goebel, G (2023) "Balloon Launches and Their Use in Weather Observations." AirVectors, https://www.airvectors.net/avbloon_5.html.

[6] National Severe Storms Laboratory. "Lightning Research." NOAA National Severe Storms Laboratory, U.S. Department of Commerce, https://www.nssl.noaa.gov/research/lightning/.

[7] Winn, W. & Moore, C. & Holmes, C. & III, L.. (1979). Electric fields in thunderclouds. FAA Florida Inst. of Technol. Workshop on Grounding and Lightning Technology

[8] Waugh, S. (2016) A BALLOON BORNE PARTICLE SIZE, IMAGING, AND VELOCITY PROBE FOR IN SITU MICROPHYSICAL MEASUREMENTS, OU PhD Dissertations

[9] Rust, W. David, and Thomas C. Marshall. "Mobile, High Wind, Balloon Launching Apparatus". Journal of Atmospheric and Oceanic Technology 6.1 (1989): 215 217. https://doi.org/10.1175/1520 0426(1989)006<0215:MHWBLA>2.0.CO;2 Web.

[10] Walden Newman, William. Commandable Cut Down and Tracking Instrument for Lightning Research, and Correlation Study Between Lightning Flash Counts and Meteorological Parameters. Master's thesis, New Mexico Institute of Mining and Technology, 2008.

[11] "Lake Effect Electrification (LEE)." Earth Observing Laboratory, University Corporation for Atmospheric Research, 2023, www.eol.ucar.edu/field_projects/lee.

[12] Steiger, S. et al. (2024) "Winter Lightning to the Lee of Lake Ontario: The Lake Effect Electrification (LEE) Field Campaign". Bulletin of the American Meteorological Society 105.11: E2026 E2046. https://doi.org/10.1175/BAMS D 23 0176.1 Web.

[13] Barth, M et al. (2015). The Deep Convective Clouds and Chemistry (DC3) Field Campaign. Bulletin of the American Meteorological Society. 96. 1281 1310. 10.1175/BAMS D 13 00290.1.

[14] Sweeney, Colm. "HORUS: High Altitude Operational Return Unmanned System." NOAA Global Monitoring Laboratory, U.S. Department of Commerce, 2021, gml.noaa.gov/news/horus_v2.html.

[15] Qiao, Dongsheng, et al. "Analysis on Snap Load Characteristics of Mooring Line in Slack Taut Process." Ocean Engineering, vol. 196, 2020, 106807. ScienceDirect, https://doi.org/10.1016/j.oceaneng.2019.106807

[16] Pfeifer, Michael. "Chapter 6 Degradation and Reliability of Materials." Materials Enabled Designs, edited by Michael Pfeifer, Butterworth Heinemann, 2009, pp. 161 187. ScienceDirect, https://doi.org/10.1016/B978 0 7506 8287 9.00006 9.

[17] Elmrabet, Nabila, and Petros Siegkas. "Dimensional Considerations on the Mechanical Properties of 3D Printed Polymer Parts." Polymer Testing, vol. 90, 2020, 106656. ScienceDirect, https://doi.org/10.1016/j.polymertesting.2020.106656.

[18] Tao, Yubo, et al. "A Review on Voids of 3D Printed Parts by Fused Filament Fabrication." Journal of Materials Research and Technology, vol. 15, 2021, pp. 4860 4879. ScienceDirect, https://doi.org/10.1016/j.jmrt.2021.10.108.

[19] Patil, Hemesh & Jeyakarthikeyan, P V. (2018). Mesh convergence study and estimation of discretization error of hub in clutch disc with integration of ANSYS. IOP Conference Series: Materials Science and Engineering. 402. 012065. 10.1088/1757 899X/402/1/012065.

[20] Bjorkman, Gordon S., Jr., et al. Mesh Convergence Studies for Thin Shell Elements Developed by the ASME Task Group on Computational Modeling. U.S. Nuclear Regulatory Commission, 2000.

[21] Federal Aviation Administration. 14 CFR Part 101: Moored Balloons, Kites, and Unmanned Free Balloons. U.S. Government Printing Office, 2023, www.ecfr.gov/current/title 14/chapter I/subchapter F/part 101.

[22] Rust, Dave. "Mobile High Wind Balloon Launch Apparatus." Notes and Correspondence, Feb. 1989.

[23] "Buoyancy and Gas." University of Tennessee Physics Problems, University of Tennessee, www.electron6.phys.utk.edu/PhysicsProblems/Mechanics/9 Gereral%20Physics/buoyancy gas.html.

[24] Newcastle University. *Equations of Motion*. Newcastle University, n.d., https://www.ncl.ac.uk/webtemplate/ask-assets/external/maths-resources/mechanics/kinematics/equations-of-motion.html.

[25] Newcastle University. *Impulse and Momentum*. Newcastle University, n.d., https://www.ncl.ac.uk/webtemplate/ask-assets/external/maths-resources/mechanics/dynamics/impulse-and-momentum.html.

[26] Wang, Xiyue, et al. "Research Progress in Polylactic Acid Processing for 3D Printing." Journal of Manufacturing Processes, vol. 112, 2024, pp. 161 178. ScienceDirect, https://doi.org/10.1016/j.jmapro.2024.01.038.

[27] Cano Vicent, Alba, et al. "Fused Deposition Modelling: Current Status, Methodology, Applications and Future Prospects." Additive Manufacturing, vol. 47, 2021, 102378. ScienceDirect, https://doi.org/10.1016/j.addma.2021.102378.

[28] Ashby, Michael F., and David R.H. Jones. "Chapter 25 Mechanical Properties of Polymers." Engineering Materials 2, 4th ed., edited by Michael F. Ashby and David R.H. Jones, International Series on Materials Science and Technology, Butterworth Heinemann, 2013, pp. 419 440. ScienceDirect, https://doi.org/10.1016/B978 0 08 096668 7.00025 5.

[29] Agarwal, Sushant, and Rakesh K. Gupta. "29 Plastics in Buildings and Construction." Applied Plastics Engineering Handbook, 2nd ed., edited by Myer Kutz, William Andrew Publishing, 2017, pp. 635 649. ScienceDirect, https://doi.org/10.1016/B978 0 323 39040 8.00030 4.

[30] Mathesen, G., Wehner, C., Merrick, J., Shirley, B., Agustsson, R., Berry, R., Diego, A., & Nanni, E. (2023). Utilization of Additive Manufacturing for the Rapid Prototyping of C Band Radiofrequency Loads. Instruments, 7(3), 23. https://doi.org/10.3390/instruments7030023

[31] "Polycarbonate (PC) Plastic: Properties, Uses, & Structure." Omnexus by SpecialChem, https://omnexus.specialchem.com/selection guide/polycarbonate pc plastic.

[32] Ozsoy, Koray & Erçetin, Ali & Çevik, Zihni. (2021). Comparison of Mechanical Properties of PLA and ABS Based Structures Produced by Fused Deposition Modelling Additive Manufacturing. European Journal of Science and Technology. 802 809. 10.31590/ejosat.983317.

[33] "Infill Patterns." Prusa3D, Prusa Research, https://help.prusa3d.com/article/infill patterns_177130.

[34] Birosz, Márton Tamás, et al. "Effect of FDM Infill Patterns on Mechanical Properties." Polymer Testing, vol. 113, 2022, 107654. ScienceDirect, https://doi.org/10.1016/j.polymertesting.2022.107654

[35] Prusament. PLA Prusament Technical Data Sheet, 10 Oct. 2021, https://prusament.com/wp content/uploads/2022/10/PLA_Prusament_TDS_2021_10_EN.pdf.

[36] "ABS." Prusa3D, Prusa Research, https://help.prusa3d.com/article/abs_2058.

[37] Prusament. Prusament PCCF Technical Data Sheet, Apr. 2023, https://prusament.com/wp content/uploads/2023/04/TDS_Prusament PCCF_2023_EN.pdf.

[38] Torricelli's Law. BYJU'S, BYJU'S, https://byjus.com/physics/torricellis-law/#:~:text=What%20is%20meant%20by%20Torricelli%27s,of%20fluid%20above%20that%20hole.

Appendix 1: Python Code

```
import pandas as pd
import matplotlib.pyplot as plt
df = pd.read_csv('ThesisFigure1.csv')
time = df['Time']
acceleration = df['Acceleration']
velocity = df['Velocity']
time1 = 0.59
time2 = 1.14
plt.figure(figsize=(14, 8))
plt.plot(time, acceleration, label='Acceleration m/s^2')
plt.plot(time, velocity, label='Velocity m/s')
plt.xlabel('Time (s)')
plt.title('Acceleration and Velocity vs Time')
plt.legend()
plt.grid()
plt.axvline(time1, linestyle='--', color='red')
plt.axvline(time2, linestyle='--', color='green')
plt.show()
```

Appendix 2: Visual Analysis

Launch Number	Taut 1	Taut 2	Comments
1	0.72	1.52	
1	0.65	1.49	
1	0.68	1.48	
1	0.7	1.51	
1	0.69	1.48	
2	0.56	1.12	
2	0.55	1.18	
2	0.71	1.21	
2	0.61	1.19	
2	0.63	1.21	
3	0.62	1.14	
3	0.66	1.06	
3	0.64	1.05	
3	0.7	1.09	
3	0.65	1.03	
4	0.43	0.96	This flight had a really short taut line 1
4	0.41	0.91	
4	0.53	1.03	
4	0.43	0.99	
4	0.47	1.01	
5	0.59	1.04	Launch tube opened on side, balloon exited weirdly
5	0.54	1.09	
5	0.56	0.99	
5	0.58	1.06	
5	0.55	1.04	
6	0.54	1.13	
6	0.6	1.15	
6	0.58	1.07	
6	0.53	1.11	
6	0.57	1.09	
7	0.54	1.17	
7	0.66	1.19	
7	0.66	1.14	
7	0.6	1.09	
7	0.61	1.09	
8	0.58	1.08	Night flight, hard to ensure exact moments
8	0.62	1.14	
8	0.59	1.05	
8	0.6	1.08	
8	0.61	1.11	

Stats

Launch Number	Segment 1	Segment 2
1	0.688	1.496
2	0.612	1.182
3	0.654	1.074
4	0.454	0.98
5	0.564	1.044
6	0.564	1.11
7	0.614	1.136
8	0.6	1.092
Total Average	0.59375	1.13925

Launch Number	Taut 1	Taut 2
1	0.0258844	0.0181659
2	0.0641872	0.0370135
3	0.0296648	0.0427785
4	0.0477493	0.0469042
5	0.0207364	0.0364692
6	0.0288097	0.0316228
7	0.0497996	0.045607
8	0.0158114	0.0342053
Total Standard Dev.	0.0353304	0.0365958

The above excel sheet displays the visual analysis carried out to ensure different time frames of the 8 individual flights. The analysis carried out discussed in Section 2.1 included recording times for 8 different flights and averaging the values to determine the most efficient values.

Appendix 3: Engineering Drawings

All engineering drawings are in IPS unless otherwise stated.

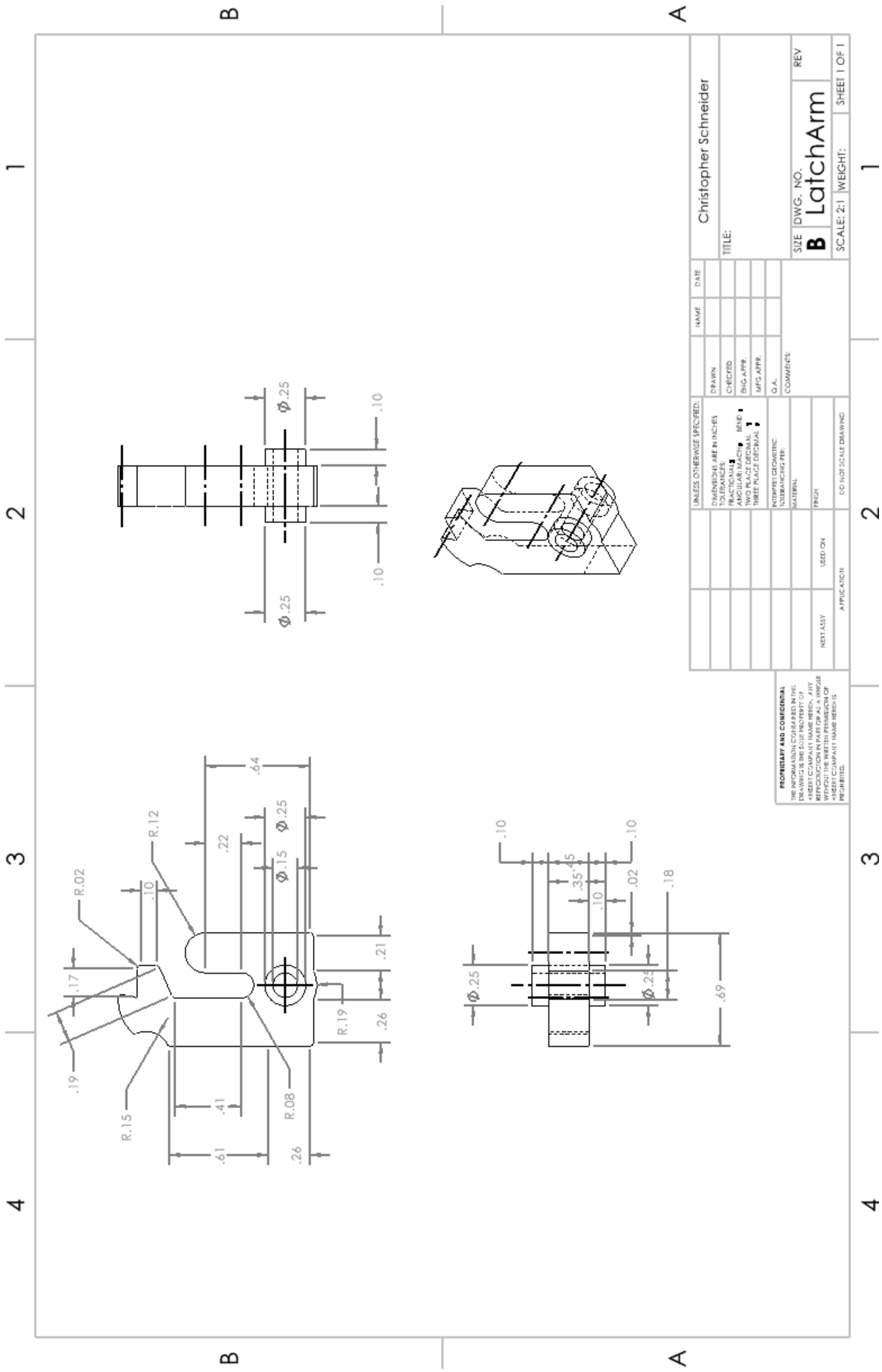

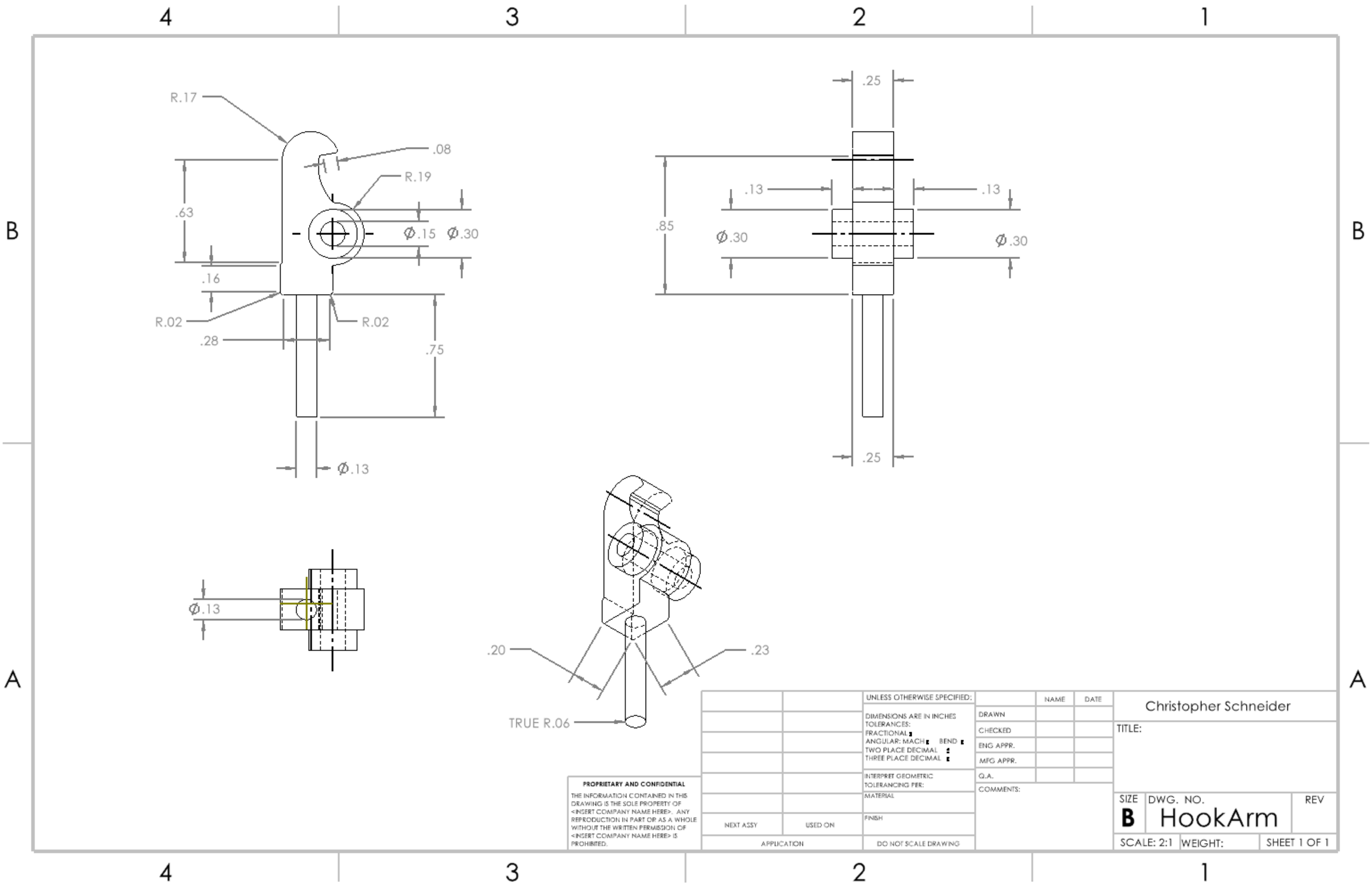

R.17
.08
R.19
.63
Ø.15
Ø.30
.16
R.02
R.02
.28
.75
Ø.13
.25
.13
.13
.85
Ø.30
Ø.30
.25
Ø.13
.20
.23
TRUE R.06
PROPRIETARY AND CONFIDENTIAL
THE INFORMATION CONTAINED IN THIS DRAWING IS THE SOLE PROPERTY OF <INSERT COMPANY NAME HERE>. ANY REPRODUCTION IN PART OR AS A WHOLE WITHOUT THE WRITTEN PERMISSION OF <INSERT COMPANY NAME HERE> IS PROHIBITED.
NEXT ASSY
USED ON
APPLICATION
UNLESS OTHERWISE SPECIFIED:
DIMENSIONS ARE IN INCHES
TOLERANCES:
FRACTIONAL
ANGULAR: MACH BEND
TWO PLACE DECIMAL
THREE PLACE DECIMAL
INTERPRET GEOMETRIC TOLERANCING PER:
MATERIAL
FINISH
DO NOT SCALE DRAWING
NAME
DATE
DRAWN
CHECKED
ENG APPR.
MFG APPR.
Q.A.
COMMENTS:
Christopher Schneider
TITLE:
SIZE
B
DWG. NO.
HookArm
REV
SCALE: 2:1
WEIGHT:
SHEET 1 OF 1

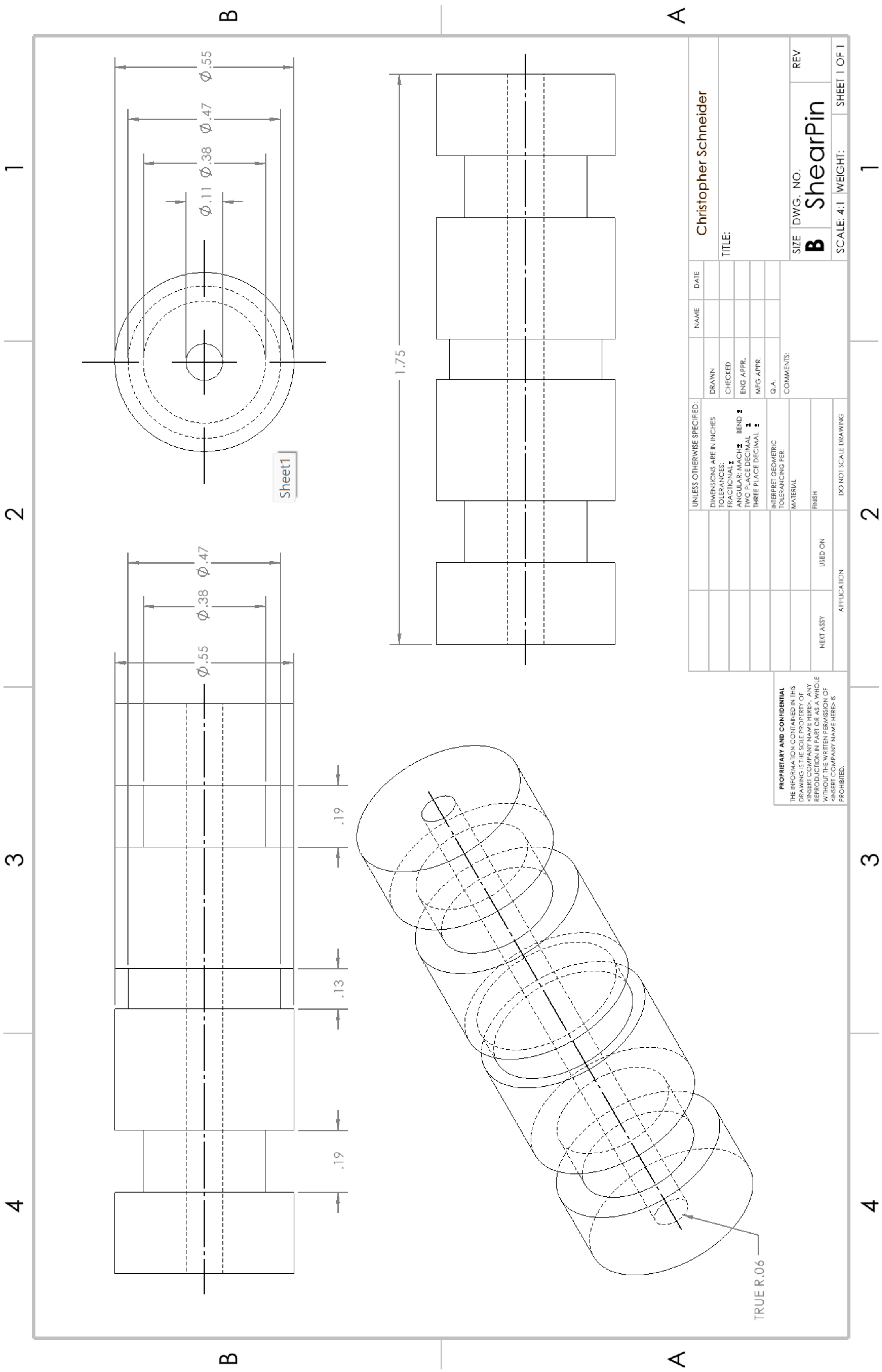
Christopher Schneider
TITLE:
SIZE B
DWG. NO.
ShearPin
REV
SCALE: 4:1
WEIGHT:
SHEET 1 OF 1
UNLESS OTHERWISE SPECIFIED:
DIMENSIONS ARE IN INCHES
TOLERANCES:
FRACTIONAL ±
ANGULAR: MACH ± BEND ±
TWO PLACE DECIMAL ±
THREE PLACE DECIMAL ±
INTERPRET GEOMETRIC TOLERANCING PER:
MATERIAL
FINISH
DO NOT SCALE DRAWING
NEXT ASSY
USED ON
APPLICATION
DRAWN
CHECKED
ENG APPR.
MFG APPR.
Q.A.
COMMENTS:
NAME
DATE
PROPRIETARY AND CONFIDENTIAL
THE INFORMATION CONTAINED IN THIS DRAWING IS THE SOLE PROPERTY OF <INSERT COMPANY NAME HERE>. ANY REPRODUCTION IN PART OR AS A WHOLE WITHOUT THE WRITTEN PERMISSION OF <INSERT COMPANY NAME HERE> IS PROHIBITED.
Ø.55
Ø.47
Ø.38
Ø.11
1.75
.19
.13
.19
TRUE R.06
Sheet1
A
B
1
2
3
4

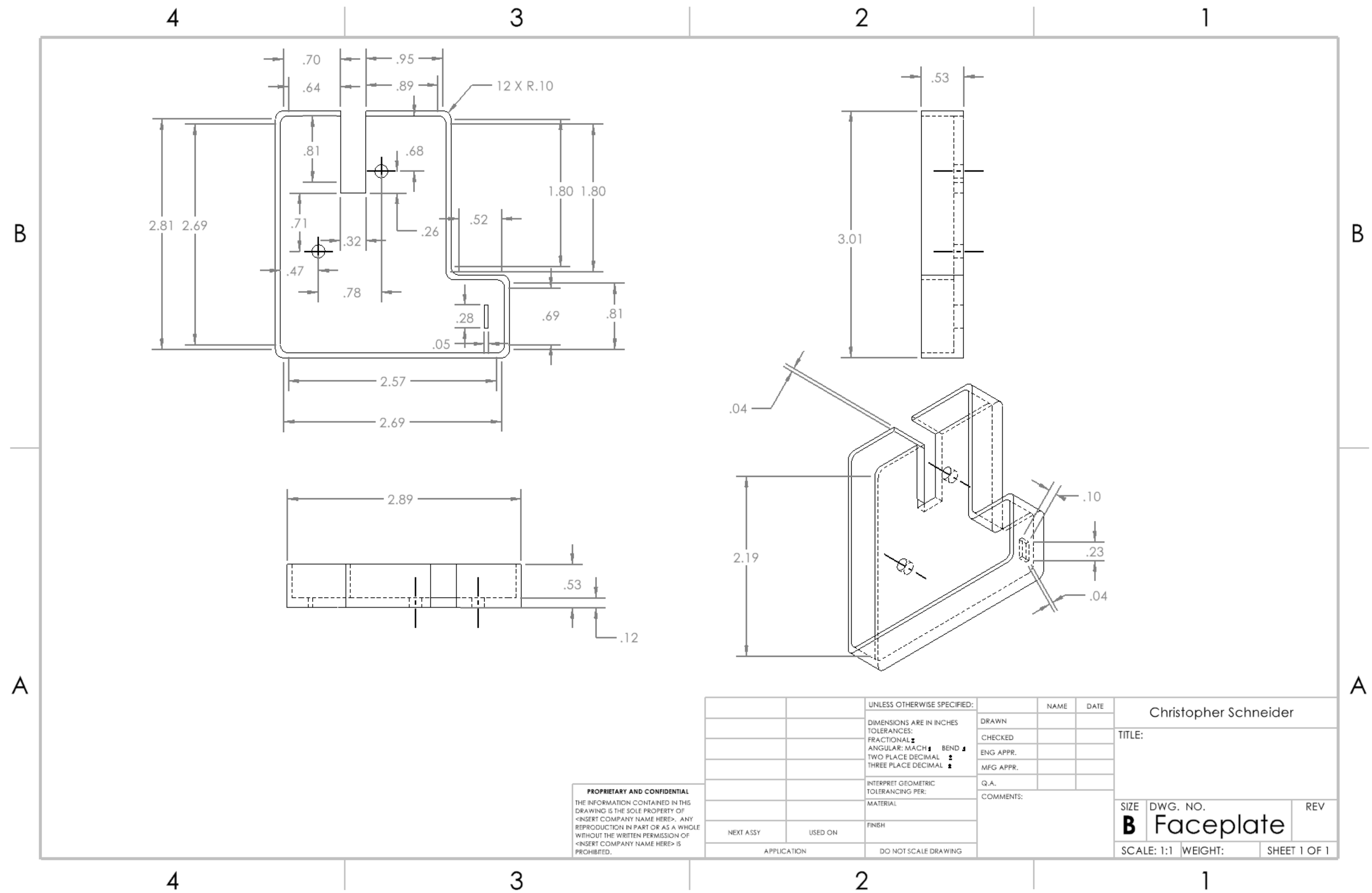
.70
.64
.95
.89
12 X R.10
.81
.68
1.80 1.80
2.81 2.69
.71
.32
.26
.52
.47
.78
.28
.69
.81
.05
2.57
2.69
2.89
.53
.12
.53
3.01
.04
.10
2.19
.23
.04
UNLESS OTHERWISE SPECIFIED:
DIMENSIONS ARE IN INCHES
TOLERANCES:
FRACTIONAL ±
ANGULAR: MACH ± BEND ±
TWO PLACE DECIMAL ±
THREE PLACE DECIMAL ±
INTERPRET GEOMETRIC TOLERANCING PER:
MATERIAL
FINISH
DO NOT SCALE DRAWING
NEXT ASSY
USED ON
APPLICATION
NAME
DATE
DRAWN
CHECKED
ENG APPR.
MFG APPR.
Q.A.
COMMENTS:
Christopher Schneider
TITLE:
SIZE
B
DWG. NO.
Faceplate
REV
SCALE: 1:1
WEIGHT:
SHEET 1 OF 1
PROPRIETARY AND CONFIDENTIAL
THE INFORMATION CONTAINED IN THIS DRAWING IS THE SOLE PROPERTY OF <INSERT COMPANY NAME HERE>. ANY REPRODUCTION IN PART OR AS A WHOLE WITHOUT THE WRITTEN PERMISSION OF <INSERT COMPANY NAME HERE> IS PROHIBITED.

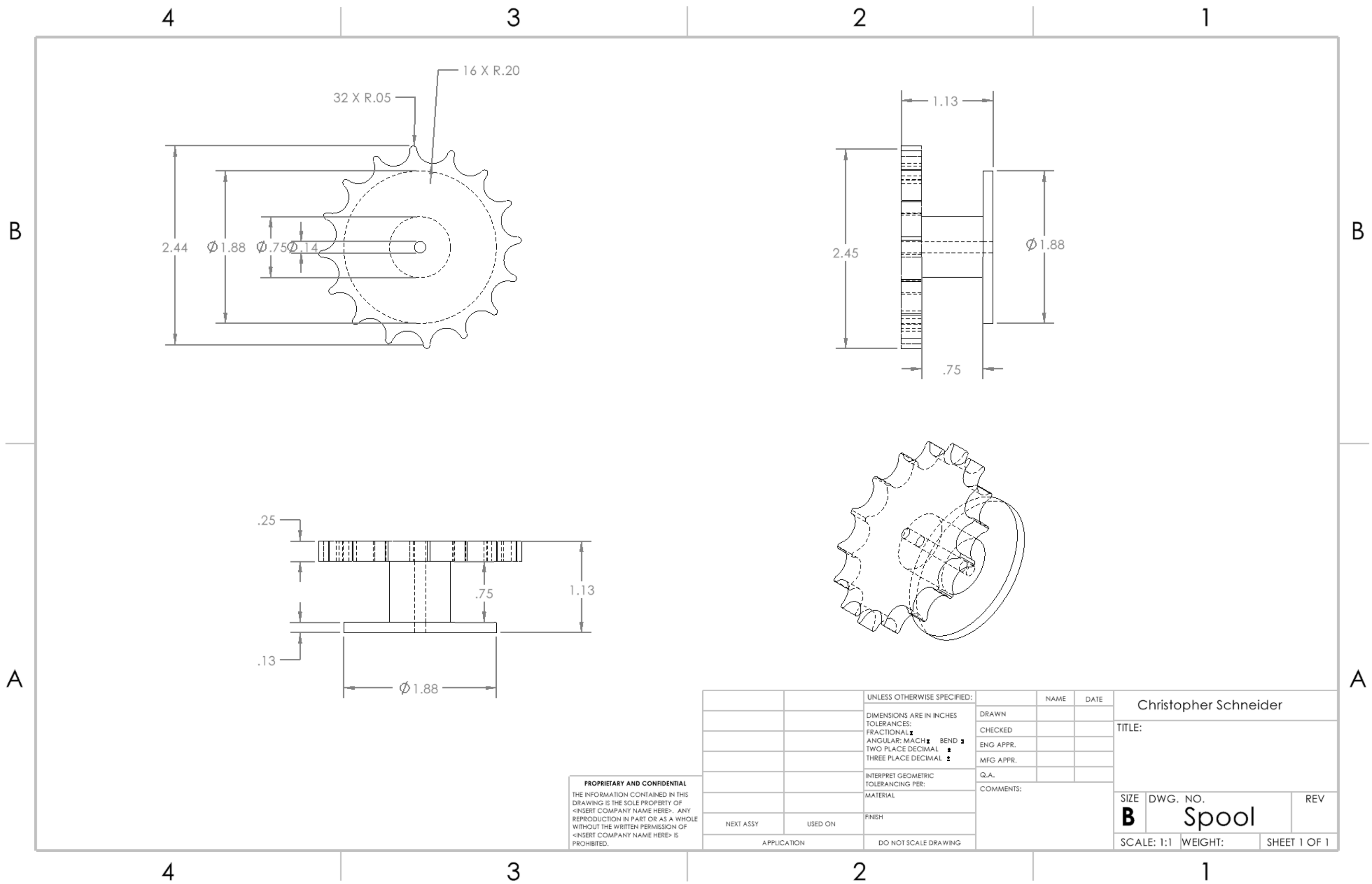
4
3
2
1
B
A
16 X R.20
32 X R.05
2.44
Ø1.88
Ø.75
Ø.14
1.13
2.45
Ø1.88
.75
.25
.75
1.13
.13
Ø1.88
PROPRIETARY AND CONFIDENTIAL
THE INFORMATION CONTAINED IN THIS DRAWING IS THE SOLE PROPERTY OF <INSERT COMPANY NAME HERE>. ANY REPRODUCTION IN PART OR AS A WHOLE WITHOUT THE WRITTEN PERMISSION OF <INSERT COMPANY NAME HERE> IS PROHIBITED.
NEXT ASSY
USED ON
APPLICATION
UNLESS OTHERWISE SPECIFIED:
DIMENSIONS ARE IN INCHES
TOLERANCES:
FRACTIONAL±
ANGULAR: MACH± BEND ±
TWO PLACE DECIMAL ±
THREE PLACE DECIMAL ±
INTERPRET GEOMETRIC TOLERANCING PER:
MATERIAL
FINISH
DO NOT SCALE DRAWING
NAME
DATE
DRAWN
CHECKED
ENG APPR.
MFG APPR.
Q.A.
COMMENTS:
Christopher Schneider
TITLE:
SIZE
B
DWG. NO.
Spool
REV
SCALE: 1:1
WEIGHT:
SHEET 1 OF 1

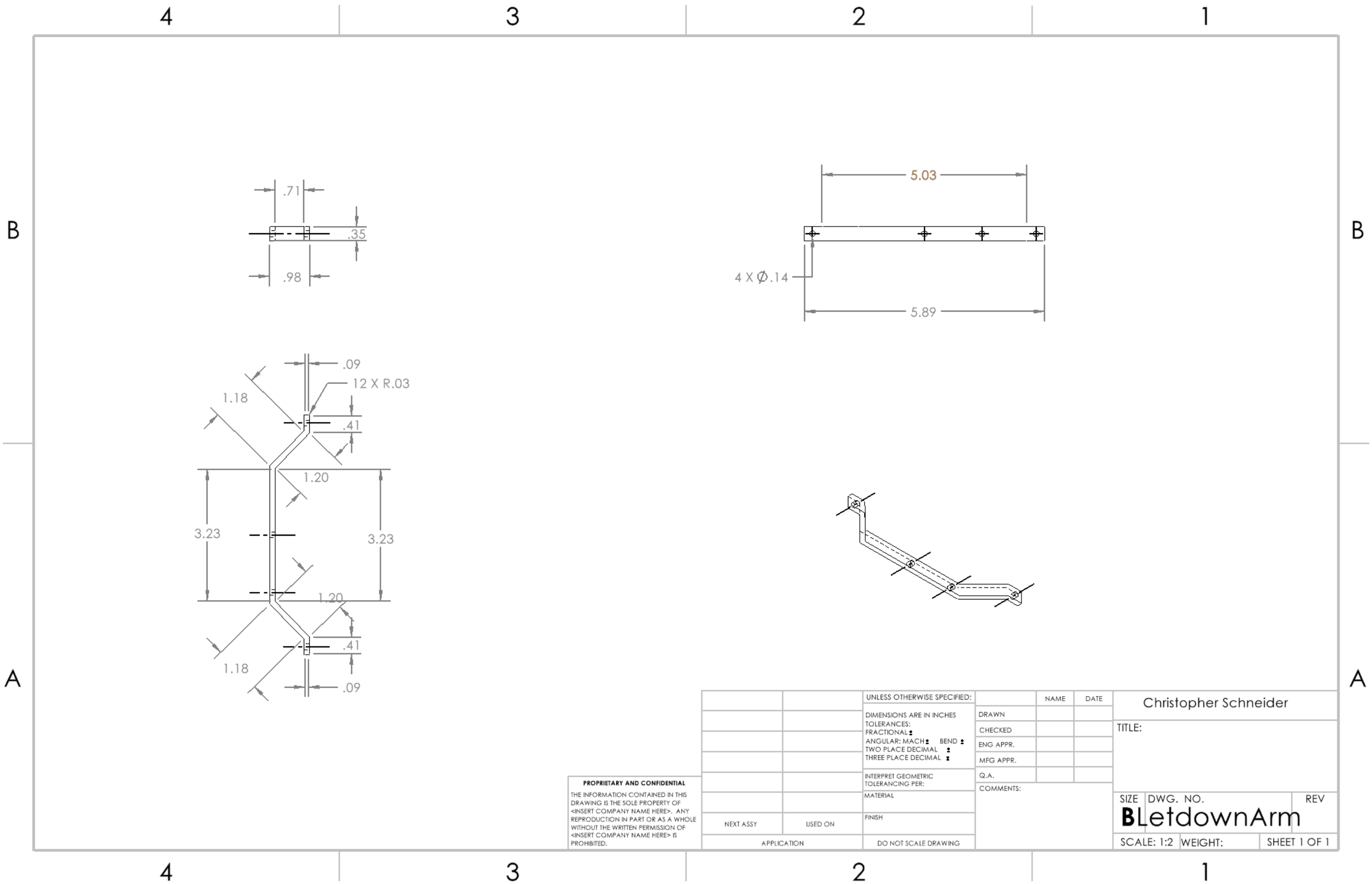

.71
.35
.98
5.03
4 X Ø.14
5.89
.09
12 X R.03
1.18
.41
1.20
3.23
3.23
1.20
.41
1.18
.09
PROPRIETARY AND CONFIDENTIAL
THE INFORMATION CONTAINED IN THIS DRAWING IS THE SOLE PROPERTY OF <INSERT COMPANY NAME HERE>. ANY REPRODUCTION IN PART OR AS A WHOLE WITHOUT THE WRITTEN PERMISSION OF <INSERT COMPANY NAME HERE> IS PROHIBITED.
NEXT ASSY
USED ON
APPLICATION
UNLESS OTHERWISE SPECIFIED:
DIMENSIONS ARE IN INCHES
TOLERANCES:
FRACTIONAL ±
ANGULAR: MACH ± BEND ±
TWO PLACE DECIMAL ±
THREE PLACE DECIMAL ±
INTERPRET GEOMETRIC TOLERANCING PER:
MATERIAL
FINISH
DO NOT SCALE DRAWING
NAME
DATE
DRAWN
CHECKED
ENG APPR.
MFG APPR.
Q.A.
COMMENTS:
Christopher Schneider
TITLE:
SIZE
DWG. NO.
REV
B
LetdownArm
SCALE: 1:2
WEIGHT:
SHEET 1 OF 1

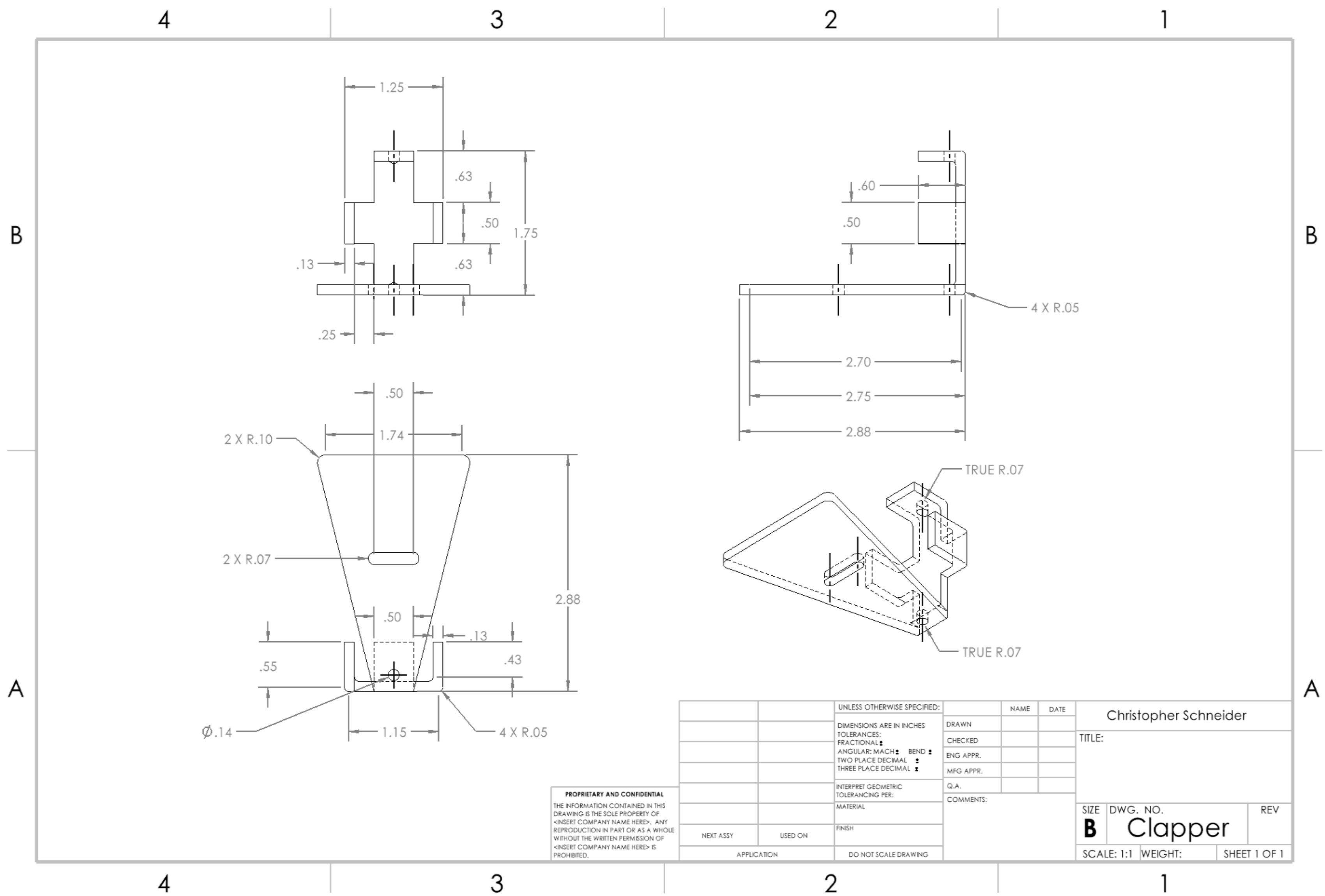

1.25
.63
.50
1.75
.13
.63
.25
.60
.50
4 X R.05
2.70
2.75
2.88
.50
2 X R.10
1.74
2 X R.07
2.88
.50
.13
.55
.43
Ø.14
1.15
4 X R.05
TRUE R.07
TRUE R.07
PROPRIETARY AND CONFIDENTIAL
THE INFORMATION CONTAINED IN THIS DRAWING IS THE SOLE PROPERTY OF <INSERT COMPANY NAME HERE>. ANY REPRODUCTION IN PART OR AS A WHOLE WITHOUT THE WRITTEN PERMISSION OF <INSERT COMPANY NAME HERE> IS PROHIBITED.
NEXT ASSY
USED ON
APPLICATION
UNLESS OTHERWISE SPECIFIED:
DIMENSIONS ARE IN INCHES
TOLERANCES:
FRACTIONAL ±
ANGULAR: MACH ± BEND ±
TWO PLACE DECIMAL ±
THREE PLACE DECIMAL ±
INTERPRET GEOMETRIC TOLERANCING PER:
MATERIAL
FINISH
DO NOT SCALE DRAWING
NAME
DATE
DRAWN
CHECKED
ENG APPR.
MFG APPR.
Q.A.
COMMENTS:
Christopher Schneider
TITLE:
SIZE
B
DWG. NO.
Clapper
REV
SCALE: 1:1
WEIGHT:
SHEET 1 OF 1